

THE PHYSICS OF HANBURY BROWN–TWISS
INTENSITY INTERFEROMETRY:
FROM STARS TO NUCLEAR COLLISIONS *

GORDON BAYM

Department of Physics, University of Illinois at Urbana-Champaign
1110 W. Green St., Urbana, IL 61801, USA

(Received April 14, 1998)

In the 1950's Hanbury Brown and Twiss showed that one could measure the angular sizes of astronomical radio sources and stars from correlations of signal intensities, rather than amplitudes, in independent detectors. Their subsequent correlation experiments demonstrating quantum bunching of photons in incoherent light beams were seminal in the development of quantum optics. Since that time the technique of "intensity interferometry" has become a valuable probe of high energy nuclear and particle collisions, providing information on the space-time geometry of the collision. The effect is one of the few measurements in elementary particle detection that depends on the wave mechanics of the produced particles. Here we discuss the basic physics of intensity interferometry, and its current applications in high energy nuclear physics, as well as recent applications in condensed matter and atomic physics.

PACS numbers: 25.75. Gz, 95.75. Kk

1. Introduction

Hanbury Brown–Twiss (HBT) interferometry, the measurement of two identical particle correlations, has become a very important technique in particle and heavy-ion collisions, enabling one to probe the evolving geometry of the collision volume. Figures 1 and 2 illustrate the general idea of an HBT measurement: plotted in Fig. 1 is the two-particle correlation function, $C(Q_{\text{inv}})$ — measured for pairs of π^+ as well as for pairs of π^- by NA44 for 200 GeV/A S on Pb at the CERN SPS [1] — as a function of the invariant momentum difference $Q_{\text{inv}} = [(p_1 - p_2)^2]^{1/2}$ of the two particles. The characteristic falloff distance Δq in momentum of the correlation function is of

* Presented at the XXXVII Cracow School of Theoretical Physics, Zakopane, Poland, May 30–June 10, 1997.

order 50 MeV/c for pions; the length $\hbar/\Delta q$, which is ~ 4 fm, is basically a measure of the size of the source of the final state pions, the size of the source when the pions no longer interact strongly with other particles. Also shown in Fig. 1, for comparison, is the correlation function for pairs of $\pi^+\pi^+$ for 450 GeV protons on Pb, which, being broader, indicates a smaller source size. Figure 2 similarly shows the correlation function for $\pi^+\pi^+$, $\pi^-\pi^-$, and K^+K^+ pairs produced in collisions of Au on Au at 10.8 GeV/A measured by E877 at the AGS in Brookhaven, also as a function of the invariant momentum difference [2].

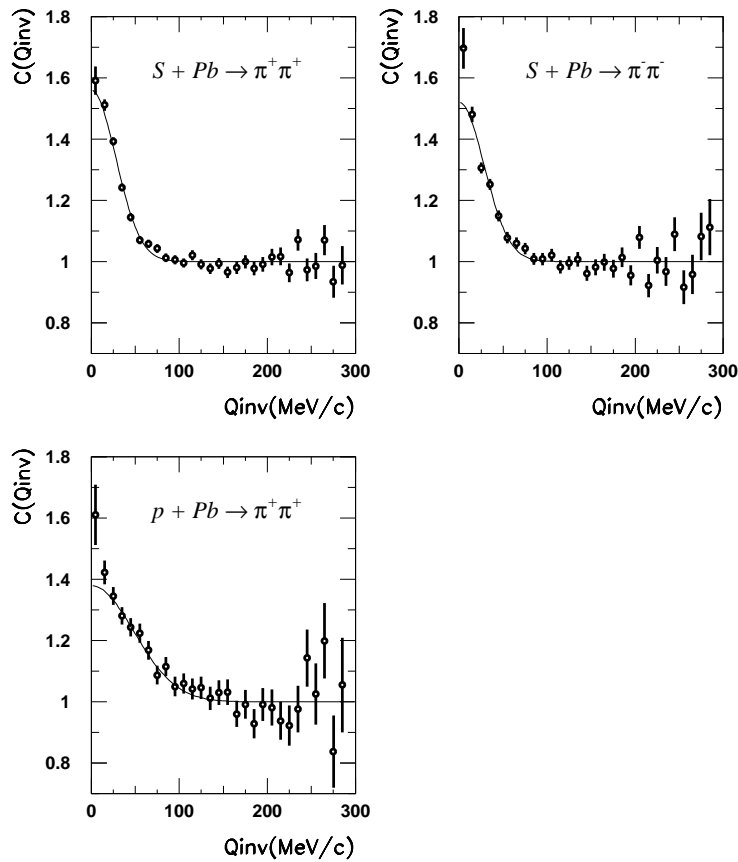


Fig. 1. Two-particle correlation function for $\pi^+\pi^+$ and $\pi^-\pi^-$ pairs in 200 GeV/A collisions of S on Pb, and $\pi^+\pi^+$ pairs in collisions of 450 GeV p on Pb [1].

In general, the two-correlation function is defined by

$$C(q) = \frac{\langle \{n_{\vec{p}_1} n_{\vec{p}_2}\} \rangle}{\langle \{n_{\vec{p}_1}\} \rangle \langle \{n_{\vec{p}_2}\} \rangle}, \quad (1)$$

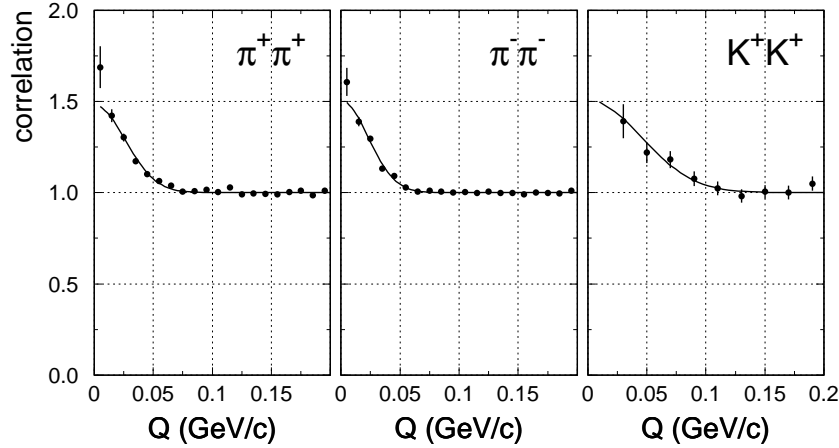


Fig. 2. Two-particle correlation function for $\pi^+\pi^+$, $\pi^-\pi^-$, and K^+K^+ pairs in collisions of Au on Au at 10.8 GeV/A [2].

where $n_{\vec{p}}$ is the number of particles of momentum \vec{p} measured in a single event, $\vec{q} = \vec{p}_1 - \vec{p}_2$, and the averages, denoted by $\langle \dots \rangle$, are over an ensemble of events. The pairs in the numerator are taken from the same event, and the pairs in the denominator from different events. Usually, one also averages the numerator and denominator separately over a range of center of mass momenta $\vec{P} = \vec{p}_1 + \vec{p}_2$ of the pair, an average denoted here by $\{ \dots \}$. As q becomes very large the correlations between the particles are lost, and the correlation function approaches unity.

The basic issue I want to discuss in these lectures is how and why HBT interferometry works. The effect is in a unique class of experiments involving multiparticle correlations that are sensitive to the actual wave mechanics of particles as they stream out to the detectors. Normally, one imagines quantum mechanics as being important in high energy experiments only until the particles leave the interaction region; from then on one usually pictures them as little bullets on classical trajectories. (Quantum phenomena such as kaon regeneration and neutrino oscillations involve the internal degrees of freedom of the particles, rather than spatial amplitudes.) Considering the wave mechanics of the emitted particles in space and time is crucial to understanding questions such as why *independent* particle detectors give a greater signal when they are close together, corresponding to small q , than far apart. Further issues are: How accurately are the distances that are determined by the falloff of the correlation function related to the size of the system? In principal the correlation function at small momenta differences should rise up to 2 for a perfectly chaotic source. However, it only goes up to ~ 1.5 – 1.6 for the pion pairs shown in Figs 1 and 2. What is the physics that

reduces the correlation function at small momentum differences? What is the effect of final state Coulomb interactions on the measured correlations?

I will begin by describing the HBT effect in the simplest model of classical waves, and then discuss how one can understand HBT in terms of the quantum mechanics of the particles reaching detectors. Then I will turn to the nuclear physics applications and finally mention applications of HBT interferometry in both atomic and condensed matter physics. My aim here is to describe the physics underlying the HBT effect. For more detailed discussions of the current experimental situation in ultrarelativistic heavy-ion collisions and its theoretical interpretation, the reader is referred to, *e.g.*, the reviews [3–8].

2. Basic model of HBT intensity interferometry

HBT interferometry differs from ordinary amplitude interferometry in that it does not compare amplitudes (as in a Young’s two-slit interferometer) but rather intensities at different points¹. The simplest picture of HBT interferometry, from which we can see the fundamental idea, is to consider two distant random point sources of light, a and b (of the same frequency), or more realistically for a star, a distribution of point sources, and imagine measuring the light falling in two independent telescopes 1 and 2; [9] see Fig. 3. The detectors are not connected by any wires. Assume that the sources are separated in space by \vec{R} , the two detectors by \vec{d} , and that the distance from the sources to the detectors, L , is much larger than R or d .

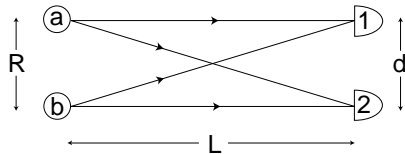


Fig. 3. Measurement of the separation of two sources, a and b , by correlation of intensities in detectors 1 and 2.

Imagine that source a produces a spherical electromagnetic wave of amplitude $\alpha e^{ik|\vec{r}-\vec{r}_a|+i\phi_a}/|\vec{r}-\vec{r}_a|$, and source b a spherical wave of amplitude $\beta e^{ik|\vec{r}-\vec{r}_b|+i\phi_b}/|\vec{r}-\vec{r}_b|$, where ϕ_a and ϕ_b are random phases (we ignore polarizations here). Let us calculate the correlation of the electromagnetic intensities in 1 and 2 as a function of the separation of the two telescopes. The total amplitude at detector 1 is

$$A_1 = \frac{1}{L} \left(\alpha e^{ikr_{1a}+i\phi_a} + \beta e^{ikr_{1b}+i\phi_b} \right), \quad (2)$$

¹ As we shall see below, there is a close connection between the two types of interferometry.

where r_{1a} is the distance from source a to detector 1, *etc.*, and the total intensity in 1 is

$$I_1 = \frac{1}{L^2} \left(|\alpha|^2 + |\beta|^2 + \alpha^* \beta e^{i(k(r_{1b}-r_{1a})+\phi_b-\phi_a)} + \alpha \beta^* e^{-i(k(r_{1b}-r_{1a})+\phi_b-\phi_a)} \right), \quad (3)$$

with a similar result for I_2 . On averaging over the random phases the latter exponential terms average to zero, and we find the average intensities in the two detectors,

$$\langle I_1 \rangle = \langle I_2 \rangle = \frac{1}{L^2} (\langle |\alpha|^2 \rangle + \langle |\beta|^2 \rangle). \quad (4)$$

The product of the averaged intensities $\langle I_1 \rangle \langle I_2 \rangle$ is independent of the separation of the detectors.

On the other hand, multiplication of the intensities $I_1 I_2$ before averaging gives an extra non-vanishing term $\sim (\alpha^* \beta)(\alpha \beta^*)$, and we find after averaging over the phases that

$$\begin{aligned} \langle I_1 I_2 \rangle &= \langle I_1 \rangle \langle I_2 \rangle + \frac{2}{L^4} |\alpha|^2 |\beta|^2 \cos(k(r_{1a} - r_{2a} - r_{1b} + r_{2b})) \\ &= \frac{1}{L^4} [(|\alpha|^4 + |\beta|^4) + 2|\alpha|^2 |\beta|^2 (1 + \cos(k(r_{1a} - r_{2a} - r_{1b} + r_{2b})))]. \end{aligned} \quad (5)$$

Then

$$C(\vec{d}) = \frac{\langle I_1 I_2 \rangle}{\langle I_1 \rangle \langle I_2 \rangle} = 1 + 2 \frac{\langle |\alpha|^2 \rangle \langle |\beta|^2 \rangle}{(\langle |\alpha|^2 \rangle + \langle |\beta|^2 \rangle)^2} \cos(k(r_{1a} - r_{2a} - r_{1b} + r_{2b})). \quad (6)$$

For large separation between the sources and detectors ($L \gg R$),

$$k(r_{1a} - r_{2a} - r_{1b} + r_{2b}) \rightarrow k(\vec{r}_a - \vec{r}_b) \cdot (\hat{r}_2 - \hat{r}_1) = \vec{R} \cdot (\vec{k}_2 - \vec{k}_1),$$

where $\vec{k}_i = k\hat{r}_i$ is the wavevector of the light seen in detector i . The correlated signal in Eq. (6) varies as a function of the detector separation d on a characteristic length scale

$$d = \lambda/\theta, \quad (7)$$

where λ is the wavelength of the light, and $\theta = R/L$ is the angular size of the sources as seen from the detectors. Thus by varying the separation of the detectors one learns the apparent angle between the two sources, and with a knowledge of the individual wavevectors, the physical size of the source.

If instead of two discrete sources, one has a distribution of sources, $\rho(\vec{r})$, then averaging over the distribution, one finds that the correlation function measures the Fourier transform of the source distribution:

$$C(\vec{d}) - 1 \sim \left| \int d^3r \rho(\vec{r}) e^{i(\vec{k}_1 - \vec{k}_2) \cdot \vec{r}} \right|^2. \quad (8)$$

One important difference between astronomical observations and high energy physics is that the stars stay fixed, while in a collision, the system evolves a time scale of 10^{-23} to 10^{-22} seconds, and thus one has to take into account the changing geometry. As we will see, in high energy physics one measures not the Fourier transform of the distribution in space alone, but to good approximation the Fourier transform in both space and time. A second important difference is that in astronomy, in the absence of a knowledge of the distance to the source, one cannot measure the actual difference in direction of the wavevectors of the light in the two detectors, and thus one measures only the angular size of the source as seen from the detectors. In a high energy experiment, one can determine the wavevectors of the detected particles, and thus measure the absolute size of the source.

To find an enhanced correlation at detector separation $\leq \lambda/\theta$ it is not necessary for the two detectors to be wired together. One needs only to compare the data trains. Why, we may ask, do two independent nearby detectors produce extra signal? Essentially if the amplitude varies randomly then a positive fluctuation of the amplitude will produce a correlated increase in both measured signals, and vice versa for a negative fluctuation. For example, in black-body radiation, both the real and imaginary parts of the complex electric fields $E \sim \alpha e^{i\vec{k} \cdot \vec{r} - i\omega t}$ are Gaussianly distributed. For independent Gaussianly distributed real variables x and y , one finds simply that $\langle (x^2 + y^2)^2 \rangle = 2\langle x^2 + y^2 \rangle^2$, so that

$$\langle |E_1|^2 |E_1|^2 \rangle = 2(\langle |E_1|^2 \rangle)^2, \quad (9)$$

while for a coherent source, *e.g.*, a laser, $\langle |E_1|^2 |E_1|^2 \rangle \simeq (\langle |E_1|^2 \rangle)^2$. The extra factor of two is precisely the source of the HBT correlations, the enhancement that arises from the cosine term in Eqs (5) and (6).

Not apparent in the simple model above is how to deal with the time involved in making measurements. For example, how far apart can one shift the data trains in time in comparing the intensities in the two detectors and still find a correlation between the signals? I will return to these questions below.

3. A brief history of the HBT effect

The radar technology developed in the Second World War opened the field of radio astronomy in the postwar period, and soon led to the discovery of bright radio “stars” in the sky. One had no idea how big various sources, *e.g.*, Cassiopeia A and Cygnus A, were, and the immediate problem was how to measure their sizes. The standard technique in use was Michelson interferometry, in which one compares the *amplitudes* of the light landing at two separated points, *e.g.*, by converging the two signals using a lens and producing a diffraction pattern as a function of the separation of the points. From the structure of the diffraction pattern (on a distance scale λ/θ) one can determine the angular size of the source. Using this technique Michelson measured the angular diameter of Jupiter’s system of moons in 1891, and K. Schwarzschild first measured the angular diameter of binary stars in 1895. The resolution by amplitude interferometry at a given wavelength is limited by the size of the separations over which one can compare amplitudes. Were the radio sources to have had a large angular size, then one would only have needed a small separation of the two detectors. On the other hand, were the sources small, then it might have been necessary to separate the telescopes by distances too large, *e.g.*, on opposite sides of the Atlantic, to be able correlate the amplitudes with the technology available in this period. This is the problem that the radio astronomer Robert Hanbury Brown at Jodrell Bank solved in 1949. His basic realization was that “if the radiation received at two places is mutually coherent, then the fluctuation in the *intensity* of the signals received at those two places is also correlated.” [10] Hanbury Brown then brought in Richard Twiss who had a more mathematical training to carry out the mathematical analysis of intensity correlations.

The first test of intensity interferometry was in 1950, when Hanbury Brown and Twiss measured the diameter of the sun using two radio telescopes operating at 2.4m wavelength (in the FM band) — quite a spectacular demonstration of the technique. Their group then went on to measure the angular diameters of the Cas A and Cyg A radio sources, which turned out to be resolvable within a few kilometers. Since they could in fact have done Michelson interferometry over such distances, Hanbury Brown described the intensity interferometry effort as “building a steam roller to crack a nut.” [11] Nowadays, Michelson interferometry has completely replaced intensity interferometry in astronomy. In radio astronomy, amplitude interferometry is the basis of the Very Large Array (VLA) in Socorro, New Mexico, and the extended VLBI, in which one compares radio amplitudes in separated radio telescopes. The 10 m optical Michelson interferometer on the Space Interferometry Mission satellite, to be flown in 2004, will be able to resolve objects to 5 microseconds of arc.

Intensity interferometry actually has an intimate relation with Michaelson amplitude interferometry, as noted by Hanbury Brown and Twiss [12]. Amplitude interferometry measures essentially the square of the sum of the amplitudes A_1 and A_2 falling on detectors 1 and 2:

$$|A_1 + A_2|^2 = |A_1|^2 + |A_2|^2 + (A_1^* A_2 + A_1 A_2^*). \quad (10)$$

The latter term in parentheses, called the “fringe visibility,” V , is the interesting part of the signal. Averaged over random variation in the signal, V^2 is simply

$$\langle V^2 \rangle = 2\langle |A_1|^2 |A_2|^2 \rangle + \langle A_1^{*2} A_2^2 \rangle + \langle A_1^2 A_2^{*2} \rangle. \quad (11)$$

As one can see from the simple model above, Eq. (2), the final terms vary rapidly on a scale of separations, $d \sim \lambda$, the wavelength of the radiation, and average to zero. On the other hand, the first term in Eq. (11) is just twice the correlation of the intensities landing in the two detectors. Thus

$$\langle V^2 \rangle \rightarrow 2\langle I_1 I_2 \rangle; \quad (12)$$

the time-average of the square of the fringe visibility is proportional to the time-averaged correlation of the intensities.

While it was well demonstrated both theoretically and experimentally that intensity interferometry worked for radio waves, which were commonly understood as classical fields, it was not obvious in the early 1950's that the effect should also work for light. Light being made of photons was more mysterious than radio signals made of classical electrical waves; the connections, now clear, were obscure at the time. Hanbury Brown and Twiss decided to test the idea for optics, with a simple tabletop experiment in which they used a beam from a mercury vapor lamp — a thermal source — and a half-silvered mirror to split the beam in two [13]. By measuring the intensity correlations between the two separated beams, they essentially compared the intensities at two different points in the unseparated beam, and by varying the relative path lengths between the mirror and the detectors they could vary the time separation, τ , of the points. What they found was that while at large τ there were no intensity correlations, the correlations increased with decreasing τ . The characteristic timescale is the *coherence time* of the beam which, in this case is essentially \hbar/T , where T is the temperature of the source. This experiment was the crucial demonstration of “photon bunching,” *i.e.*, that photons in a seemingly uncorrelated thermal beam tend to be detected in close-by pairs. Their results were greeted with great disbelief, and various experiments were done to disprove them. In the end Hanbury Brown and Twiss prevailed, aided by a particularly important

paper by Purcell [14] which showed how to understand the effect in terms of electric field fluctuations (see Eq. (9)) — and the field of quantum optics was born.

Armed with the demonstration that intensity interferometry worked for light, Hanbury Brown and Twiss then went on to apply the technique to measure the angular size of the star Sirius (α Canus Majoris A) by studying optical intensity correlations between two telescopes [15]. Since the telescopes required good light gathering ability but not great resolution, Hanbury Brown and Twiss were able to fashion a pair from five-foot diameter searchlights left over from the Second World War. The signals from the two telescopes were correlated electronically (although the actual physical connection is not needed to observe the effect). Figure 4 sketches their data for the correlation function $C(d) - 1$, divided by its value at $d=0$, measured as a function of the separation d of the two telescopes out to a maximum separation ~ 9 m. The data yielded an angular diameter of Sirius of $0.0068'' \pm 0.0005'' = 3.1 \times 10^{-8}$ radians, a very impressive measurement of an object at a distance of 2.7 pc. The four data points shown were taken for a total of some 18 hours over a 5 month period, an indication of the poor viewing conditions. The dashed line is the expected curve for a uniformly illuminated disk of angular diameter, $0.0063''$.

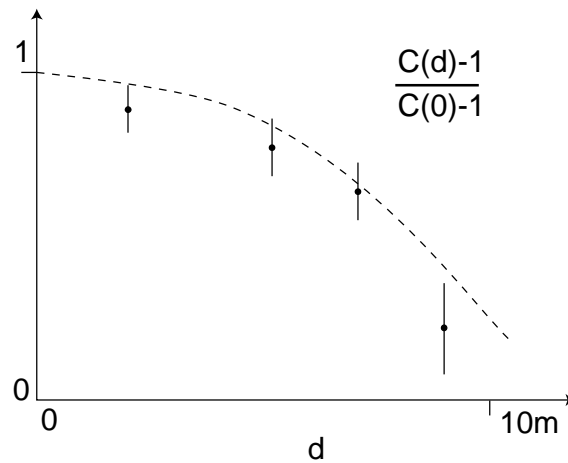


Fig. 4. Measurement of the angular diameter of Sirius [15]

This figure looks very similar in structure to the heavy-ion plots in Figs 1 and 2. An important difference is that the actual HBT correlation seen here was just one part in 10^6 , a tiny signal above the background. What is the source of this difference? The question is whether all observed pairs of

photons are “HBT-correlated”²; for example, if one takes a data train from 1956 in one telescope and compares it with a data train in the other from 1997 will one see interferometry? The answer is that the photons are in fact HBT-correlated only if they are emitted within a coherence time, the characteristic timescale in the original HBT tabletop experiment with an optical source. For a star the coherence time is $\tau_{\text{coh}} \sim 10^{-14}$ sec. On the other hand, the signal was studied over a band 5–45 MHz, corresponding to a binning time $\tau_{\text{bin}} \sim 10^{-8}$ sec. Roughly the probability of observing an HBT-correlated pair of photons is $\sim \tau_{\text{coh}}/\tau_{\text{bin}} \sim 10^{-6}$. Figure 5 shows the region where photons produce an HBT signal in the plane of the times, t_1 and t_2 , of detections in detectors 1 and 2. Below we discuss the analogous timescales in heavy-ion collisions.

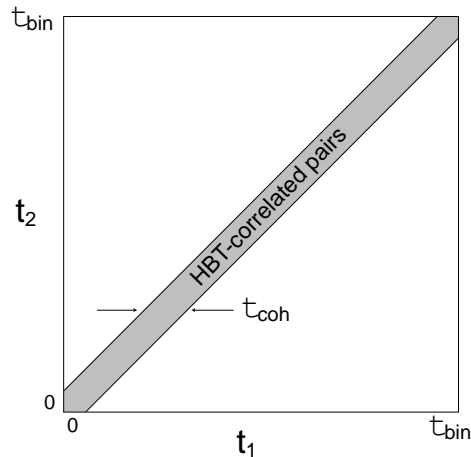


Fig. 5. Region in the plane of the detection times $t_1 - t_2$ where photon pairs produce an HBT signal.

4. Quantum mechanics of HBT

The simple derivation of intensity interferometry in Sec. 2 is entirely classical. How can one understand the effect from a quantum mechanical viewpoint? If we think of the sources a and b in Fig. 3 as emitting photons, we can identify four different processes, shown in Fig. 6: (i) source a

² Here we mean correlated in the sense that the photon pairs will produce an HBT effect at the detectors, measured by C , as opposed to the different question of the correlations in the beam produced in the source, as discussed in Sec. 6. The language is potentially confusing, since photons that are maximally correlated at the source, *e.g.*, in a laser beam, do not exhibit an HBT effect, while a thermal source, which is minimally correlated, produces the maximum HBT effect.

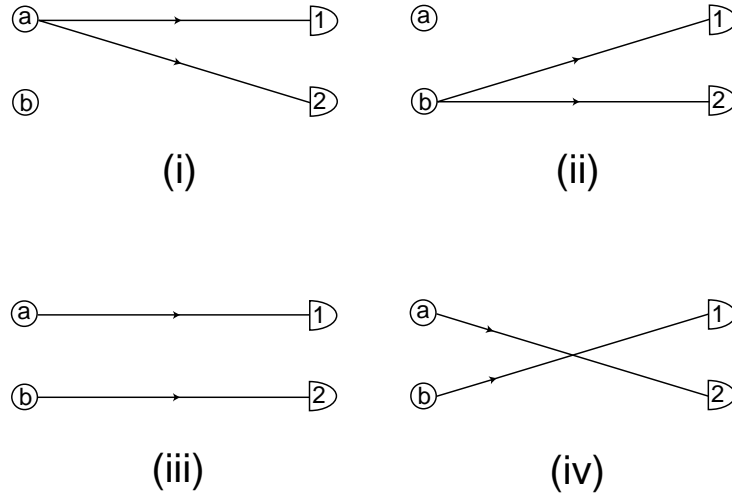


Fig. 6. The four independent photon emission and detection processes included in Eq. (5).

emits two photons, one detected in each detector, (ii) source b emits the two photons instead; (iii) source a emits a photon detected in 1 and b emits a photon detected in 2, and finally, (iv) source a emits a photon detected in 2 and b emits a photon detected in 1, the exchange of the previous process, (iii). The first two processes are distinguishable, and do not produce any interferometry. They simply correspond to detection of the sources independently (the $|\alpha|^4$ and $|\beta|^4$ terms in Eq. (5)). Only the latter two processes, (iii) and (iv), which are quantum-mechanically coherent, give rise to interferometry. [Indeed, if we drop the terms proportional to $|\alpha|^4$ and $|\beta|^4$, then Eq. (6) reduces to $C(\vec{d}) = 1 + \cos(k(r_{1a} - r_{2a} - r_{1b} + r_{2b}))$.] Quantum mechanically, the HBT effect is a consequence of ordinary boson exchange, an effect included in the symmetry of the wave function of the pair of particles, *e.g.*, for a pair of independent bosons in orthogonal states ϕ_α and ϕ_β , $\phi(1, 2) = (\phi_\alpha(1)\phi_\beta(2) + \phi_\alpha(2)\phi_\beta(1)) / \sqrt{2}$. The effect is present for all pairs of identical bosons, including pions and kaons produced in high energy collisions.

The detection of interferometry in particle collisions dates from 1960 when G. Goldhaber, S. Goldhaber, W.Y. Lee, and A. Pais [16] studied angular correlations of pions produced in $p\bar{p}$ collisions at the Bevatron. According to Pais [17], the idea of exploring interferometry in particle physics, although so similar to that in astronomical observations, was independently conceived. The method is now a standard technique in high energy collisions, from heavy ions [3–8], to meson–nucleon interactions [18], to electron–positron annihilation [19]. As noted by Feynman [20], the experiment done

with electrons would yield intensity anti-correlations. However the effect is obscured by interactions among the fermions; electron pairs or proton pairs have a repulsive Coulomb interaction which itself decreases the correlation function at small momentum differences (see Sec. 9), while neutrons at small relative momenta have significant final state strong interactions. Correlation studies of nucleon pairs produced in heavy-ion collisions are described in Refs [5] and [21], and references therein. HBT interferometry is now being applied in study of boson atomic beams as well [22], as we discuss in Sec. 10.

Eventually, we will describe HBT measurements in terms of the two-particle correlation functions of the emitted identical particles. It is more intuitive, however, first to study the problem in terms of particle wave functions. To be specific we focus on pions, although the discussion is quite general.

How does one describe quantum mechanically the set of pions emitted emitted in a nuclear collision? Even in the best of all possible worlds — where one knows the exact wave function of the two colliding nuclei, and knows exactly how the quantum mechanical evolution operator does its job to produce the final system as a coherent superposition of well defined pure quantum mechanical states $\Psi(1, 2, \dots, N)$ of N particles — the subset of pions emitted is described by a *mixed* quantum state. Quite generally, any subset of particles in a pure state is described by a mixed state, even, *e.g.*, for the electron in the ground state of a freely moving hydrogen atom. The single particle density matrix for pions of a given charge at equal time is given by

$$\langle \pi^\dagger(r, t) \pi(r', t) \rangle = \int d^3r_2 \cdots d^3r_n \Psi^*(r, r_2, \dots, r_N, t) \Psi(r', r_2, \dots, r_N, t), \quad (13)$$

where $\pi(x)$ is the operator destroying a pion of the given charge at point $x = (\vec{r}, t)$.

If Ψ is a product of single particle wave functions, then $\langle \pi^\dagger(x) \pi(x') \rangle$ factors into a product of single particle states, $\phi^*(x) \phi(x')$. In general the single-pion correlation function does not factor, even when the pions are no longer interacting, but it can be represented as a sum over a collection of single particle states ϕ_i :

$$\langle \pi^\dagger(x) \pi(x') \rangle = \sum_i f_i \phi_i^*(x) \phi_i(x'), \quad (14)$$

where the f_i give the probability of finding the pion in single particle state i . For example, the probability of finding a pion at point 1 is given by

$\sum_i f_i |\phi_i(1)|^2$. Only if the pion part of the state Ψ factors out in the form of a product of the same single particle states for all the pions — a Bose–Einstein condensate — will single pions be in a pure state. The mixed single pion state always has finite entropy, $-\sum_i (f_i \ln f_i - (1 + f_i) \ln(1 + f_i))$.

The closest one can come to describing pions as little bullets is to picture the single particle states making up the mixed ensemble of pions as wavepackets with almost well defined momenta and energies, limited by the uncertainty principle. We picture the collision volume as made up of many sources of pions; whether the sources are fragmentation of strings, or in the language of low energy nuclear physics individual nucleon–nucleon collisions, the sources are localized to within a distance R which is less than the size of the entire collision volume, and the emission process is temporally localized to within a time τ . Thus the individual components of momentum, \vec{p} , and energy, ε_p , of the emitted particles are uncertain to within

$$\begin{aligned} \Delta p_a &\gtrsim \frac{\hbar}{R}, \quad a = x, y, z \\ \Delta \varepsilon_p &\gtrsim \frac{\hbar}{\tau}. \end{aligned} \tag{15}$$

A pion nominally of momentum \vec{p} emitted from a source at the origin in space and time would have an amplitude to have four-momentum $q = (\varepsilon_q, \vec{q})$ that is roughly Gaussian,

$$A(q) \sim e^{-(\vec{q}-\vec{p})^2 R^2/2} e^{-(\varepsilon_q-\varepsilon_p)^2 \tau^2/2}, \tag{16}$$

and in space-time the particle would be described by a wavepacket

$$\phi_{\vec{p}}(x) = \int \frac{d^3q}{(2\pi)^3} \frac{e^{iqx}}{2\varepsilon_q} A(q). \tag{17}$$

How does the packet evolve in time after leaving the source? Assume that the collision takes place, and the particles emerge, into vacuum. (In real life secondary scattering on other atoms in the target and also scattering in air are both very important effects, to which we return in Sec. 8.) The transverse spatial spread, perpendicular to \vec{p} , is determined by the uncertainty in transverse velocity, which for relativistic particles ($\varepsilon_p \approx p$) is:

$$\Delta v_{\perp} = \frac{\Delta p_{\perp}}{\varepsilon_p} \sim \frac{1}{pR}. \tag{18}$$

The spread in longitudinal velocity is

$$\Delta v_L = \Delta \left(\frac{p_L}{\varepsilon_p} \right) = \frac{\Delta p_L}{\gamma^2 \varepsilon_p} \sim \frac{1}{\gamma^2 pR}, \tag{19}$$

where $\gamma = \varepsilon_p/m$ is the Lorentz factor, and m is the pion mass. The presence of the factor γ^2 reflects the fact that the more relativistic the particles become the closer to the speed of light the packet moves, with vanishing spread in longitudinal velocity. The transverse size of the wavepacket after travelling a distance L is thus $\sim L/pR$, while its thickness is $\sim L/\gamma^2 pR$.

To be specific, consider a 1 GeV pion ($\gamma = 7$) produced within an initial radius of 10 fm travelling to a detector 10 meters from the source. Then the transverse spread of the wavepacket is about 20 cm, while the thickness of the packet grows to half a centimeter. Pions emerge in rather extended pancake-like states. The characteristic time for such a pion wavepacket to cross a point at the distance of the detector is $\sim 10^{-11}$ sec. Smaller source sizes lead to even larger spreads in the pion wavepackets. Photons would have a similar transverse spread; however, the thickness of the wavepacket would not grow.

5. Detector response

Let us now turn to the question of the detection of particles in such wavepacket states by a magnetic spectrometer. In the ‘‘bullet’’ picture, the particle travels along a classical trajectory, excites an atom in the detector, which determines the direction of its momentum, and begins to make a track (or in emulsion makes a spot on photographic film); the particle continues on, producing a curved track in the spectrometer, from which one deduces the magnitude of its momentum. But, in fact, the particle has a distribution of probability amplitudes, wherever its wavepacket ϕ is non-zero, of where it makes the first spot in the spectrometer. A particle of mean momentum \vec{p} can, because of the transverse momentum uncertainty, be detected anywhere within the range of momenta Δp_\perp around \vec{p} contained in its wavepacket. After the initial collision in the detector, a much more narrowly focused wave packet emerges. (If one does not actually do the measurement, the state that emerges is a mixed state corresponding to all possible points where the incident packet can excite a detector atom.) The narrowed packet continues through the magnetic field, and the subsequent collisions it makes selects its energy. One measures momentum by measuring a sequence of positions in the detection.

Consider the measurement of the momentum of an incident particle in state $\phi_i(x)$. The probability that it makes the first single excitation of an atom in the detector at point A and continues to produce a track corresponding to measuring its momentum to be \vec{k} is then

$$P_{\vec{k}}(A; i) = \int dx dx' e^{ikx} \phi_i^*(x) s_A(x, x') e^{-ikx'} \phi_i(x'). \quad (20)$$

Here the detector atom response function, s , is localized in r and r' about the atom at A ; it also extends over an interval in $t - t'$ which is the characteristic time that the detector analyzes the amplitude and phase variation of the incident wave, of order 10^{-16} sec $\sim \hbar/(10$ eV), the inverse of a characteristic atomic excitation energy. This time is much shorter than the typical nanosecond scale resolution time of a detector, the time it takes to build up a million-fold cascade of electrons³. More generally, the probability of detection of a pion of given charge at A is given by

$$P_{\vec{k}}(A) = \int dx dx' e^{ik(x-x')} s_A(x, x') \langle \pi^\dagger(x) \pi(x') \rangle, \quad (21)$$

where $\langle \pi^\dagger(x) \pi(x') \rangle$ is the single-pion correlation function.

Consider next the detection of two independent particles. The question is why, if one detector lights up, do nearby detectors tend to have greater probability to light up than detectors further away — the HBT effect. Suppose first that the two particles are incident in orthogonal wavepackets ϕ_i and ϕ_j . The symmetrized two-particle wave function is $\phi(\vec{r}, \vec{r}', t) = (\phi_i(\vec{r}, t)\phi_j(\vec{r}', t) + \phi_i(\vec{r}', t)\phi_j(\vec{r}, t)) / \sqrt{2}$. The probability of a joint detection by a detector atom at A of a pion that continues to make a track corresponding to momentum \vec{k} , and by a detector atom at B of a second pion that continues to make a track corresponding to momentum \vec{k}' , is then given by

$$\begin{aligned} P_{\vec{k}, \vec{k}'}(A, B; i, j) &= \int dx dx'' e^{ik(x-x'')} s_A(x, x'') \int dx' dx''' e^{ik'(x'-x''')} s_B(x', x''') \\ &\quad \times (\phi_i(x)\phi_j(x') + \phi_i(x')\phi_j(x))^* (\phi_i(x'')\phi_j(x''') + \phi_i(x''')\phi_j(x'')) \\ &= P_{\vec{k}}(A; i)P_{\vec{k}'}(B; j) + P_{\vec{k}}(A; j)P_{\vec{k}'}(B; i) \\ &\quad + \mathcal{A}_{\vec{k}}(A; i, j)\mathcal{A}_{\vec{k}'}(B; j, i) + \mathcal{A}_{\vec{k}}(A; j, i)\mathcal{A}_{\vec{k}'}(B; i, j), \end{aligned} \quad (22)$$

where

$$\mathcal{A}_{\vec{k}}(C; i, j) = \int dx dx'' e^{ik(x-x'')} s_C(x, x'') \phi_i^*(x) \phi_j(x''). \quad (23)$$

The first term in Eq. (22) is the probability of the particle in state i being detected at A times the probability of the particle in state j being detected at B , and the second is the same with i and j interchanged. These are the normal terms.

³ A detailed discussion of the role of the detectors is given in Popp's thesis [23], and in Ref. [24].

The final two terms in Eq. (22) are the enhancement of the detection probability — the HBT effect. As we see, in order to have enhancement, it is necessary that both wavepackets, i and j , overlap in the detector at A during the time that the detector is doing quantum mechanics on the incoming system, and similarly that they also must overlap in the detector at B (but note that the wavepackets do not have to be present in both detectors simultaneously). The presence of the wavepackets simultaneously in each of the detectors is the reason the detectors produce more signal when they are close to each other⁴.

The maximum transverse separation d of the detectors that will produce an HBT signal is essentially the transverse size of a given wavepacket, L/pR , the wavelength divided by the angular size of the source as seen from the detectors, where again L is the distance from the source to the detector, R is the size of the source, and p is the average particle momentum. The scale of relative momenta q for which one finds a signal is $q/p = d/L \sim 1/pR$, and thus $q \sim 1/R$, the standard HBT result. As we see from this argument, the HBT effect directly measures the width of the wavepackets at the first detection. This width is in turn determined by the uncertainties in the momentum distribution at the time that the wavepacket is no longer affected by strong interactions with the other particles in the collision.

Generally the amplitudes, Eqs (16) and (17), of the wavepackets, $A(q)$, vary slowly in q on an atomic scale, $\sim 1 \text{ KeV}/c$. In this case the overlap integral (23) is not sensitive to the detection time scales, $\sim 10^{-16}$ sec, and one finds a correlation function:

$$C(p, p') = 1 + \frac{|\sum_i f_i A_i^*(p) A_i^*(p')|^2}{\sum_i f_i |A_i(p)|^2 \sum_j f_j |A_j(p')|^2}, \quad (24)$$

where f_i is the single pion probability in the ensemble, Eq. (14).

However, if a particle is delayed in emission by more than the detection time scale, the HBT correlations between that particle and one produced directly will be suppressed. A simple example in heavy-ion collisions of this effect is in the correlation of π^- produced in Λ decay, $\Lambda \rightarrow \pi^- + p$, with directly produced pions. Because the Λ travels more slowly than a directly produced pion of the same rapidity as one emitted in the decay, the pion from decay will lag the directly produced one by a time Δt . To

⁴ Imagine that the detection at A occurs before the detection at B . Then one may ask how both original wavepackets can be at the second detector, since the first detection “reduces” the wavepacket of the detected particle. From this point of view the amplitude for detection of a particle at B is proportional to the amplitude, $\phi_j(B)$, for it to be in state j at B times the amplitude, $\phi_i(A)$, for the other particle in state i to have been detected earlier at A , plus the same product with $i \leftrightarrow j$. The resulting joint probability is the same as Eq. (22). I thank J. Walcher for raising this question.

estimate this effect, we note that a π^- emitted in the forward direction has rapidity $y_\pi^0 \approx 0.67$ in the Λ frame, and that a Λ of rapidity y travels on average a distance $\tau_\Lambda \sinh y$ before decaying, where τ_Λ is the Λ lifetime. Thus $\Delta t = \tau_\Lambda / (\cosh y + \sinh y / \tanh y_\pi^0)$, which for a Λ of typical rapidity 3 is $\sim 0.037\tau_\Lambda = 9.7 \times 10^{-12}$ sec, much longer than the detector timescale. Pions emitted in other than the forward direction will have an even greater time lag.

As the above discussion makes apparent, the enhanced signal is not a consequence of special preparation at the source, such as a particle of a given momentum inducing emission of other particles of similar momentum, as in a laser. (In fact, a coherent source such as a laser would not give an HBT signal.) Clearly, in the stellar case there can be no such connection between emission processes on opposite sides of the star, and yet photons from opposite sides give an HBT enhancement. The effect is a property of the detection. Furthermore, if two stars, S and T , which are at very different distances from the Earth, are approximately along the same line of sight, Fig. 7(a), one will see HBT correlations between a photon from S and a photon from T . Of course the emission times have to be different in order that the two photons arrive at each of the detectors at the same time. (Even in measuring a single star one correlates earlier emitted photons from the stellar rim with later emitted photons from the front surface.) The HBT correlations between photons from the two sources as a function of detector separation, d , sketched in Fig. 7(b), would have an oscillatory term characteristic of the angular separation of the two stars (*cf.* Eq. (6)), modulated by a broader Gaussian characteristic of the angular size of an individual star. By comparison, a single bright star, T , surrounded by a halo of dim stars (an average over a distribution of stars S), would yield a correlation function, Fig. 7(c), with a rise proportional, for $d \lesssim d_2$, to the inverse of the angular size of the central star λ/d_2 , plus a much more narrow rise, for $d \lesssim d_1$, inversely proportional to the angular size of the halo. As an exercise, sketch the correlation function produced by two lasers which are mutually incoherent, rather than the two stars.

That the HBT effect is not a property of production, but rather is a property of detection is well illustrated by the following experiment. Imagine, as in Fig. 8, that RHIC, the BNL heavy-ion collider, sends a pion into a far away particle detector array, and that by using the pionic analog of a half-silvered mirror, we reflect a pion from CERN into the same detector array, so that it arrives at the same time as the pion from RHIC. As long as the wavepackets of the pions overlap sufficiently that the interference amplitudes \mathcal{A} at the detector atoms are non-zero, one will see an HBT enhancement! As this experiment illustrates, the HBT effect does not depend on the history of the particles. What matters is the form of the wavepackets when they arrive at the detectors.

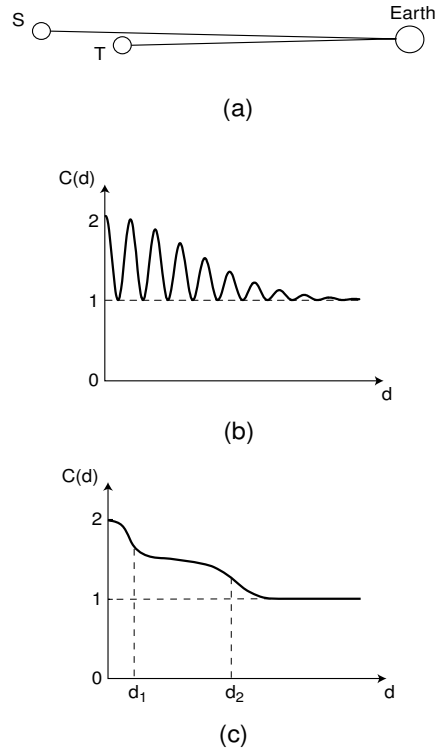


Fig. 7. (a) Two stars, S , and T , along nearby lines of sight from the earth; (b) schematic of HBT measurement of correlated intensity from the two stars; (c) schematic of HBT measurement a bright star surrounded by a halo of dim stars.

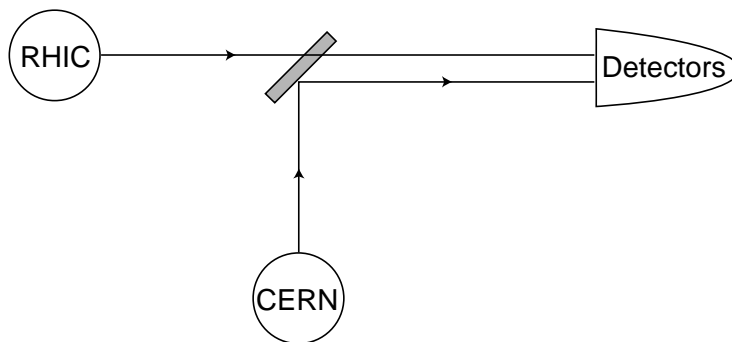


Fig. 8. Detection of the HBT effect between a pion from RHIC and a pion from CERN.

6. Correlation functions

Let us now turn to describing the HBT effect in terms of the correlations of the sources of pions in a collision. To generalize Eq. (22), we may write the joint probability of detection at the detectors at A and B in terms of the two-pion correlation function $\langle \pi^\dagger(x)\pi^\dagger(x'')\pi(x''')\pi(x') \rangle$ as

$$\begin{aligned}
 P_{\vec{k},\vec{k}'}(A,B) &= \int dx dx' e^{ik(x-x')} s_A(x,x') \int dx'' dx''' e^{ik'(x''-x''')} s_B(x'',x''') \\
 &\times \langle \pi^\dagger(x)\pi^\dagger(x'')\pi(x''')\pi(x') \rangle.
 \end{aligned}
 \tag{25}$$

The two-pion correlation function $\langle \pi^\dagger(1)\pi^\dagger(2)\pi(3)\pi(4) \rangle$, where the integers stand for space-time points, is the amplitude for starting in a state of the system, removing a pion at 4, then removing a second pion at 3, adding a pion back at 2, adding another back at 1, and returning to the initial state.

Consider first a system of N free bosons that is completely Bose–Einstein condensed, or the photons produced by a laser. For such a system all the particles, or photons, are in the same particle state $\phi(x)$. Then the correlation function completely factors. The amplitude for removing a particle at a given point 4 is simply proportional to the wave function ϕ at the point, while the amplitude for adding a particle is proportional to ϕ^* at the point. In this case the single-particle correlation function is

$$\langle \pi^\dagger(1)\pi(2) \rangle = N\phi^*(1)\phi(2)
 \tag{26}$$

and

$$\begin{aligned}
 \langle \pi^\dagger(1)\pi^\dagger(2)\pi(3)\pi(4) \rangle &= N^2\phi^*(1)\phi^*(2)\phi(3)\phi(4) \\
 &= \langle \pi^\dagger(1)\pi(4) \rangle \langle \pi^\dagger(2)\pi(3) \rangle.
 \end{aligned}
 \tag{27}$$

Such a source is *coherent*⁵.

The correlations of particles from a thermal source, *e.g.*, a black-body cavity, are quite different. For free particles, the mean number of particles of energy ε is given by $\langle n_\varepsilon \rangle = 1/(e^{\beta(\varepsilon-\mu)} - 1)$, while the fluctuations are given by

$$\langle n_\varepsilon^2 \rangle - \langle n_\varepsilon \rangle^2 = \langle n_\varepsilon \rangle (1 \pm \langle n_\varepsilon \rangle),
 \tag{28}$$

where the upper sign is for bosons and the lower for fermions. (The fermion result follows trivially since n can only equal 0 or 1.) Translated back into a

⁵ Taking Poisson statistics for the distribution of the number n of photons in a laser beam more carefully into account leads to the same result (27), since $\langle n(n-1) \rangle = \langle n \rangle^2$.

statement about the correlation function, one finds the expected factorized form for a thermal ensemble:

$$\langle \pi^\dagger(1)\pi^\dagger(2)\pi(3)\pi(4) \rangle = \langle \pi^\dagger(1)\pi(4) \rangle \langle \pi^\dagger(2)\pi(3) \rangle \pm \langle \pi^\dagger(1)\pi(3) \rangle \langle \pi^\dagger(2)\pi(4) \rangle, \quad (29)$$

where π here represents either a Bose or Fermi field. This equation says that if one removes two particles at 4 and 3, one can come back to the same state by either replacing the first with a particle at 1 and the second at 2 (first term), or the first at 2 and the second at 1 (second term). In the boson case, when $3 = 4$ and $1 = 2$, the amplitude for removing two particles is just $2\langle \pi^\dagger(1)\pi(4) \rangle^2$. The extra fluctuations — the factor of 2 here, or more generally the second term on the right side of Eq. (29) — are the source of the HBT interferometry effect. The maximum HBT effect occurs when the correlation function factorizes in this fashion. Then one describes the source as *chaotic*.

The source need not be thermal to factor this way. The result (29) always holds for non-interacting fermions, while for bosons it is sufficient that no single particle mode i be macroscopically occupied, *i.e.*, that all $\langle n_i \rangle \ll 1$. The basic reason one expects the correlation function in heavy-ion collisions to factorize as in Eq. (29) is that the pions undergo considerable rescattering in the hot environment of the collision volume; the key is the destruction by rescattering of phase correlations among the pions from the production process⁶.

It is useful to relate the pion correlation functions to correlations of the sources of the pion field. The freely propagating field $\pi(x)$ measured at the detector is produced according to the field equation

$$(\square^2 - m_\pi^2)\pi(x) = J(x), \quad (30)$$

where $J(x)$ is the source of the field at the last collision. Then

$$\pi(x) = \int dx' D(x, x') J(x') = \int \frac{d^3k}{(2\pi)^3} \frac{e^{ikx}}{2i\varepsilon_k} \int dx' e^{-ikx'} J(x'), \quad (31)$$

where D is the free pion Green's function, and the latter form holds in the far field. The single pion correlation function is related to the source correlation function by

$$\langle \pi^\dagger(x)\pi(x') \rangle = \int dx'' dx''' D^*(x, x'') D(x', x''') \langle J^\dagger(x'') J(x''') \rangle. \quad (32)$$

⁶ A simple example that violates Eq. (29) are the correlations among pions radiated by a weakly interacting gas of nucleons.

Generally $\langle \pi^\dagger(x)\pi(x') \rangle$ can be written in a factorized form as a sum of wavepackets as in Eq. (14).

The measured singles distribution of pions is then given in terms of the source correlation function by

$$\varepsilon_p \frac{d^3n}{d^3p} = \frac{d^3n}{d^2p_\perp dy} = \frac{1}{2} \int dx dx' e^{ip(x-x')} \langle J^\dagger(x)J(x') \rangle, \quad (33)$$

and the measured pair distribution by

$$\begin{aligned} \varepsilon_p \varepsilon'_p \frac{d^6n}{d^3p d^3p'} &= \frac{1}{4} \int dx dx' e^{ip(x-x')} dx'' dx''' e^{ip'(x''-x''')} \langle J^\dagger(x)J^\dagger(x'')J(x''')J(x') \rangle. \end{aligned} \quad (34)$$

In the following let us assume a chaotic source, so that

$$\begin{aligned} \langle J^\dagger(x)J^\dagger(x'')J(x''')J(x') \rangle &= \langle J^\dagger(x)J(x') \rangle \langle J^\dagger(x'')J(x''') \rangle + \langle J^\dagger(x)J(x''') \rangle \langle J^\dagger(x'')J(x') \rangle; \end{aligned} \quad (35)$$

then the pair distribution function becomes

$$\begin{aligned} \varepsilon_p \varepsilon'_p \frac{d^6n}{d^3p d^3p'} &= \frac{1}{4} \int dx dx' dx'' dx''' e^{ip(x-x')} e^{ip(x''-x''')} \\ &\quad \times \langle J^\dagger(x)J(x') \rangle \langle J^\dagger(x'')J(x''') \rangle \\ &\quad \times \left[e^{ip(x-x')} e^{ip'(x''-x''')} + e^{ip(x-x''')} e^{ip'(x''-x')} \right]. \end{aligned} \quad (36)$$

We see that the HBT correlation function, defined by

$$C(q) = \frac{d^6n/d^3p d^3p'}{(d^3n/d^3p)(d^3n/d^3p')}, \quad (37)$$

where $\vec{q} = \vec{p} - \vec{p}'$ (and with implied separate averages over the center of mass coordinates of the numerator and denominator, *cf.* Eq. (1)), measures the structure of the current-current correlation function. Note that the information it provides is on the nature of the source of particles after the last strong interactions, when the particles begin to stream freely towards the detectors.

The correlation function $\langle J^\dagger(x)J(x') \rangle$ contains two length, and time, scales. The range of the center of mass variables, $X = (\vec{r} + \vec{r}')/2$, $(t + t')/2$, are on the order of the size of the collision volume, $R \sim 10$ fm, and the

duration of the collision, τ , also on the order of 5–10 fm/c. On the other hand, the dependences in $x - x'$ measure the space-time extent of the region in which the phase at a point x' is coherent with the phase of the current at x , a region of size, ξ_c and τ_c in space and time. The lengths ξ_c and τ_c , which determine the falloff of the singles distribution, Eq. (33), are typically on the order of one fm in space and one fm/c in time, much shorter than the range in the center of mass variables.

Such behavior is illustrated by the factorized form for $\langle J^\dagger(x)J(x') \rangle$,

$$\langle J^\dagger(x)J(x') \rangle = e^{-(\bar{r}+\bar{r}')^2/8R^2} e^{-(t+t')^2/8\tau^2} g(x-x'). \quad (38)$$

The singles distribution, from Eq. (33), is then

$$\varepsilon_p \frac{d^3n}{d^3p} \sim \int dx e^{ipx} g(x), \quad (39)$$

and the two-particle correlation function, assuming a chaotic source, is

$$C(q) = 1 + e^{-\bar{q}^2 R^2} e^{-q^0 \tau^2} \frac{(d^3n/d^3K)^2}{(d^3n/d^3(K+q/2))(d^3n/d^3(K-q/2))}, \quad (40)$$

where $K = (p+p')/2$. As we see from this equation, the length measured in HBT is modified from the length, R , governing the center of mass behavior of the current-current correlation function, $\langle J^\dagger(x)J(x') \rangle$, due to the final factor, the ratios of the singles distributions.

A particularly simple and illustrative model is the following. Assume that the particle production is described by a distribution of sources of size R_s, τ_s , at space-time points x_s , each producing pions in wavepackets of mean momentum \vec{p} ,

$$\phi_p(x-x_s) = \int \frac{d^3k}{(2\pi)^3} \frac{e^{ik(x-x_s)}}{2\varepsilon_k} e^{-(p-k)^2 R_s^2/2}, \quad (41)$$

with probability $f(\vec{p})$. The spread in momenta in the individual states $\phi_p(x)$ is of order \hbar/R_s . If the sources are Gaussianly distributed in space and time over a region of size R_0, τ_0 , then from Eq. (14) the pion correlation function is,

$$\begin{aligned} & \langle \pi^\dagger(x)\pi(x') \rangle \\ & \sim \int \frac{d^3p}{(2\pi)^3} f(p) \int d^4x_s e^{-r_s^2/2R_0^2} e^{-t_s^2/2\tau_0^2} \phi_p^*(x-x_s) \phi_p(x'-x_s). \end{aligned} \quad (42)$$

Carrying out the x_s integrals explicitly, one readily finds that this model is the same as that with a source of the form (38), where

$$R^2 = R_0^2 + R_s^2/2, \quad \tau^2 = \tau_s^2 + \tau_0^2/2, \quad (43)$$

and

$$g(x) = \int \frac{d^3p}{(2\pi)^3} f(p) e^{-ipx} e^{-x^2/4R_0^2}. \tag{44}$$

The details of the individual wavepackets are all subsumed in the current-current correlation function. As this model illustrates, the length scale describing the center of mass of the current correlation function is the size of the distribution of sources, plus a correction from the size of the individual sources.

In fact, this latter correction is countered by the correction from the singles distributions in Eq. (40). If we assume, solely as a mathematically simple example, that $d^3n/d^3K \sim e^{-\xi^2 K^2}$, then

$$C(q) = 1 + e^{-\bar{q}^2(R_0^2+(R_s^2-\xi^2)/2)} e^{-q^0{}^2(\tau_s^2+\tau_0^2/2)}. \tag{45}$$

The net deviations of the measured scales R and τ from the scales of the source distributions R_0 and τ_0 are of order of a few percent at most.

More generally one can define a total-momentum dependent pair source function,

$$S_P(X) = \int dx e^{-iPx/2} \langle J^\dagger(X+x/2) J(X-x/2) \rangle, \tag{46}$$

where $P = p + p'$ is the total four-momentum of the pair. For the simple example (38), we have $S_P(X) = e^{-X^2/2R^2} g(P/2)$; note the relation to the description (42) in terms of wavepackets produced by the source. In terms of S , the HBT correlation function becomes [25],

$$C(q) = 1 + \frac{|\int dX e^{iqX} S_P(X)|^2}{\int dX S_{P+q/2}(X) \int dX S_{P-q/2}(X)}. \tag{47}$$

This equation relates the HBT correlation function to four-dimensional Fourier transforms of the source function $S_P(x)$. Compare with the result (24), which gives the correlation function in terms of the Fourier transforms of the wavepackets making up the pion distribution.

The simplest approximation is to take $\xi_c = \tau_c = 0$, or equivalently, to ignore the P dependence in $S_P(X)$. Then the current-current correlation becomes a function of only one variable:

$$\langle J^\dagger(x) J(x') \rangle \rightarrow S(x) \delta(x - x'). \tag{48}$$

This approximation is excellent for stars, where the emission of a photon is coherent on the order of an atomic scale, while the size of the star is $\sim 10^{11}$

cm. Neglecting the correlation length is not as good an approximation in a heavy-ion collision.

With the neglect of the finite size of the correlation lengths, we find from Eq. (33) that

$$\varepsilon_p \frac{d^3 n}{d^3 p} = \frac{1}{2} \int dx S(x), \quad (49)$$

i.e., the singles distribution is flat in momentum. Furthermore the pair distribution (assuming a chaotic source) becomes

$$\varepsilon_p \varepsilon_{p'} \frac{d^6 n}{d^3 p d^3 p'} = \left| \frac{1}{2} \int dx S(x) \right|^2 + \left| \frac{1}{2} \int dx S(x) e^{i(p-p')x} \right|^2, \quad (50)$$

and

$$C(q) = 1 + \frac{|\int dx S(x) e^{iqx}|^2}{|\int dx S(x)|^2}. \quad (51)$$

7. Parametrizations of data

The most straightforward way to analyze HBT data is to parametrize the correlation function $C(q)$ as a Gaussian in q . Expanding $C(q)$ in Eq. (47) for small q to second order we find

$$C(q) = 2 - q^\mu q^\nu (\langle X_\mu X_\nu \rangle - \langle X_\mu \rangle \langle X_\nu \rangle) + q^\mu q^\nu (\langle x_\mu x_\nu \rangle - \langle x_\mu \rangle \langle x_\nu \rangle) + \dots, \quad (52)$$

where

$$\langle \theta(x, X) \rangle = \frac{\int dx dX \theta(x, X) \langle J^\dagger(X + x/2) J(X - x/2) \rangle}{\int dx dX \langle J^\dagger(X + x/2) J(X - x/2) \rangle}. \quad (53)$$

The terms in x in (52), which come from expansion of the denominator in Eq. (47), are of relative order $(\xi_c/R)^2$, $(\tau_c/\tau)^2$, and are often neglected in the interpretation of the data, although, as mentioned, they can modify the extracted sizes by a few percent. Dropping these latter terms we have

$$C(q) = 2 - q^\mu q^\nu (\langle x_\mu x_\nu \rangle - \langle x_\mu \rangle \langle x_\nu \rangle) + \dots, \quad (54)$$

where here and below we write $\langle \theta(x) \rangle = \int dx S_P(x) \theta(x) / \int dx' S_P(x')$. This form suggests a parametrization [26, 27],

$$C(q) = 1 + \lambda e^{-q^\mu q^\nu (\langle x_\mu x_\nu \rangle - \langle x_\mu \rangle \langle x_\nu \rangle)}, \quad (55)$$

where we also introduce the *chaoticity parameter* λ ; for a completely chaotic source the correlation function rises up to 2 as $q \rightarrow 0$, and thus $\lambda = 1$, while for a completely coherent source, such as a laser, $\lambda = 0$.

Various increasingly sophisticated versions of this parametrization have been adopted. The simplest is to write

$$C(q) = 1 + \lambda e^{-Q_{\text{inv}}^2 R^2}, \quad (56)$$

where Q_{inv} is the invariant momentum difference of the two particles, $Q_{\text{inv}}^2 = (\vec{p}_1 - \vec{p}_2)^2 - (\varepsilon_{p_1} - \varepsilon_{p_2})^2$. Results of such a single-size analysis by NA44 for pairs of π^+ and pairs of π^- produced in 200 GeV/A collisions of S on Pb at the SPS [1] are shown in Fig. 1, and by E877 for pairs of π^+ , pairs of π^- , and pairs of K^+ produced in collisions of 10.8 GeV/A Au on Au at the AGS [2] in Fig. 2. This parametrization corresponds to the assumption that $\langle x_\mu x_\nu \rangle - \langle x_\mu \rangle \langle x_\nu \rangle = g_{\mu\nu} R^2$. Since the sign of the contribution of the time-time component should be the same as the space-space components a somewhat better single-size parametrization would be to assume that $\langle x_\mu x_\nu \rangle - \langle x_\mu \rangle \langle x_\nu \rangle = \delta_{\mu\nu} R^2$. Then

$$C(q) = 1 + \lambda e^{-(\vec{q}^2 + q^0{}^2)R^2}; \quad (57)$$

cf. Eq. (45).

A second level of approximation is to distinguish the space and time dependence of the evolving system, taking a spherical fireball in space, so that

$$C(q) = 1 + \lambda e^{-(\vec{q}^2 R^2 + q^0{}^2 \tau^2)}. \quad (58)$$

The time τ is essentially the duration of the collision: $\tau^2 = \langle t^2 \rangle - \langle t \rangle^2$, and R the radius of the collision volume: $R^2 = \langle \vec{r}^2 \rangle - \langle \vec{r} \rangle^2$.

The next level is to try to take the evolving geometry into account, including non-sphericity of the source and possible flow effects. Consider a pair of particles of total three-momentum \vec{P} and relative three-momentum \vec{q} . Since $q \cdot P = (p - p') \cdot (p + p') = p^2 - p'^2 = 0$, we have

$$q^0 = \vec{q} \cdot \vec{P} / P^0 = \vec{q} \cdot \vec{v}, \quad (59)$$

where \vec{v} is the velocity of the center of mass of the pair of particles, \vec{P} / P^0 . Then $q^\mu x_\mu = \vec{q} \cdot (\vec{r} - \vec{v}t)$, and

$$q^\mu q^\nu (\langle x_\mu x_\nu \rangle - \langle x_\mu \rangle \langle x_\nu \rangle) = \langle (\vec{q} \cdot (\vec{r} - \vec{v}t))^2 \rangle - \langle \vec{q} \cdot (\vec{r} - \vec{v}t) \rangle^2. \quad (60)$$

Let us erect a three dimensional coordinate system in which the *longitudinal* direction is along the beam axis, the *outwards* axis (the x direction) is along

the transverse component of \vec{P} , and the third, or *side*, axis is in the y direction. In this frame v_y vanishes. (Note that this coordinate system varies with the pair of particles studied.) The ensemble of events is symmetric under $y \rightarrow -y$, so that cross terms involving a single y vanish. However, the cross terms $\langle zt \rangle - \langle z \rangle \langle t \rangle$ and $\langle xt \rangle - \langle x \rangle \langle t \rangle$ are generally non-zero, and we find

$$\begin{aligned} & q^\mu q^\nu (\langle x_\mu x_\nu \rangle - \langle x_\mu \rangle \langle x_\nu \rangle) \\ &= q_{\text{out}}^2 (\langle (x - v_x t)^2 \rangle - \langle x - v_x t \rangle^2) + q_{\text{side}}^2 (\langle y^2 \rangle - \langle y \rangle^2) \\ & \quad + q_{\text{long}}^2 (\langle (z - v_z t)^2 \rangle - \langle z - v_z t \rangle^2) \\ & \quad + 2q_{\text{out}} q_{\text{long}} (\langle (x - v_x t)(z - v_z t) \rangle - \langle x - v_x t \rangle \langle z - v_z t \rangle), \end{aligned} \quad (61)$$

a form which suggests a parametrization of the correlation function in terms of four radii [28],

$$C(\vec{q}) = 1 + \lambda e^{-(q_{\text{out}}^2 R_{\text{out}}^2 + q_{\text{side}}^2 R_{\text{side}}^2 + q_{\text{long}}^2 R_{\text{long}}^2 + 2q_{\text{out}} q_{\text{long}} R_{\text{ol}}^2)}, \quad (62)$$

where the parameters have the interpretation

$$\begin{aligned} R_{\text{out}}^2 &= \langle (x - v_x t)^2 \rangle - \langle x - v_x t \rangle^2, \\ R_{\text{side}}^2 &= \langle y^2 \rangle - \langle y \rangle^2, \\ R_{\text{long}}^2 &= \langle (z - v_z t)^2 \rangle - \langle z - v_z t \rangle^2, \\ R_{\text{ol}}^2 &= \langle (x - v_x t)(z - v_z t) \rangle - \langle x - v_x t \rangle \langle z - v_z t \rangle. \end{aligned} \quad (63)$$

Note that R_{ol}^2 , although written as a square, need not be positive. It is often convenient to analyze data, pair-by-pair, in the ‘‘longitudinal center of mass’’ frame, in which $P_z = 0$; then $q_{\text{out}} = q^0/v$, and R_{long}^2 reduces to $\langle z^2 \rangle - \langle z \rangle^2$.

The *three-dimensional* parametrization, Eq. (63), is commonly used in interpreting present HBT measurements. Typical three-dimensional analyses of correlations of pion pairs are shown in Figs 9 and 10, in Fig. 9 correlations of $\pi^+\pi^+$ from 200 GeV/A S+Pb collisions studied by NA44 [29], and in Fig. 10 correlations of $\pi^+\pi^+$ and $\pi^-\pi^-$ from 10.8 GeV/A Au+Au collisions studied by E877 [30].

Considerable information on the development of the collision volume, *e.g.*, flow [31], can be extracted from the three-dimensional analyses. The experimental dependence of the two-particle correlations on the momenta of the particles indeed indicates that the systems are expanding. For detailed discussions of the physics extracted from recent experiments, see, *e.g.*, Refs [32] and [33].

Figure 11 shows NA44 data on K^+K^+ and K^-K^- correlations, projected as functions of q_{long} and the component q_{transv} of \vec{q} perpendicular to the beam axis [3]. Note that the chaoticity parameter λ is somewhat larger for kaons than pions, a point which examine in the following section.

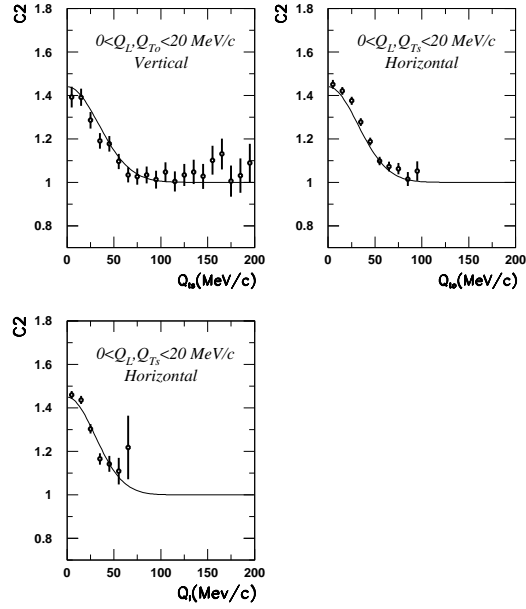


Fig. 9. Three-dimensional fittings of $\pi^+\pi^+$ correlation functions, from NA44 [29], the upper left panel as a function of q_{side} , the upper right as a function of q_{out} , and the lower panel as a function of q_{long} .

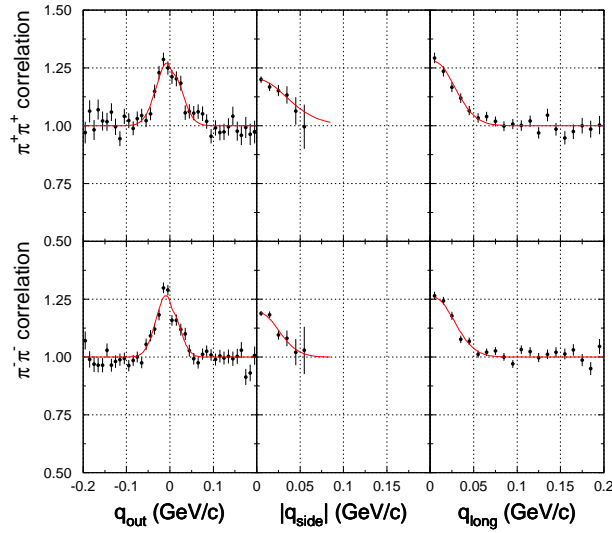


Fig. 10. Three-dimensional fittings of $\pi^+\pi^+$ and $\pi^-\pi^-$ correlation functions, from E877 [30].

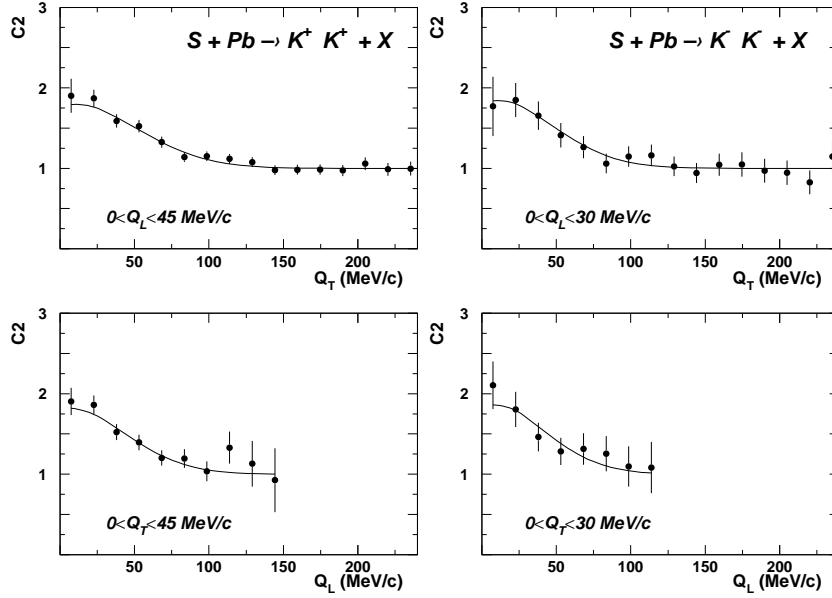


Fig. 11. Two-dimensional fittings of $K^+ K^+$ (left panels) and $K^- K^-$ (right panels) correlation functions, as functions of q_{transv} and q_{long} . From Ref. [3].

8. Sources of chaoticity $\lambda < 1$

The chaoticity parameter, λ , is generally found experimentally to be less than one, a reflection of intrinsic physical effects as well as experimental difficulties. The most fundamental effect would be that the source exhibits a level of coherence, the situation in a laser, or a form of pion or other boson condensate. HBT measurements of pions produced from a disordered chiral condensate in an ultrarelativistic heavy-ion collision would also show a reduced λ [34]. However, as we noted above, rescattering by other particles in the collision volume tends to destroy phase correlations from the production process. Another example is the MIT atom laser [35] where magnetically trapped and evaporatively cooled sodium atoms are extracted in coherent states from a Bose–Einstein condensed system; since the extracted atoms do not exhibit an HBT effect, λ would be zero. (See the discussion of HBT in atomic beams below.)

Even if the source is completely chaotic, measurements do not necessarily give $\lambda = 1$. The first reason is the simple but important problem of contamination of the sample from misidentification of particles, *e.g.*, an e^- or K^- as a π^- , so that one includes pairs of non-identical particles in the data set.

A second stems from unravelling the effects of Coulomb final state interactions between a pair of identical charged particles. The point is that the methods of removing effects of Coulomb interactions, which we discuss in some detail in the following section, become more uncertain the smaller the relative momentum difference, leading to uncertainty in λ .

The next physical effect reducing λ is the production of pions from long-lived resonances. Such pions appear to come from sources of large radii, which would give an HBT enhancement only at very small q . Indeed, perhaps half of the pions produced in an ultrarelativistic heavy-ion collision come from resonances, rather than being produced directly. Pions from short-lived resonances, *e.g.*, from $\rho \rightarrow \pi\pi$ or from $\Delta \rightarrow N\pi$, are produced well within the collision volume and are not an issue. On the other hand, the long-lived resonance η has a lifetime of order $1.2 \text{ \AA}/c$, and the 3π into which it decays would appear to be produced at a relatively enormous distance of order \AA from the collision volume. The ω goes some 24 fm, the η' some 800 fm, *etc.* The result is that the collision volume is surrounded by a halo of pions from resonances.

A small chaotic source would lead to a broad HBT correlation function, while a very large source would lead to a correlation function with a sharp rise only at small relative momenta. Now if one has both a small and a large source, *e.g.*, a partially transparent cloud in front of the sun, one sees a combination of both, as illustrated in Fig. 7(c), where the width of the bump closest to the origin is inversely proportional to the size of the large source (the cloud), and the width of the broader bump reflects the size of the small source (the sun). Figure 12 illustrates how pions from different resonances contribute to the correlation function, here as a function of the *out* component of the momentum difference, in a central CERN S–Pb collision [36]. The estimate is based on an RQMD simulation of the collision. Note the rise at very small relative momenta from long-lived resonances⁷. However, unless one is capable of resolving the little peak at small q one would deduce that the data goes to a value of λ less than one. The effect on the observed λ is a reduction of $\sim 30\%$ for pions, and $\sim 10\%$ for kaons, since a smaller fraction of kaons are produced by long-lived resonances. Since the production of resonances falls off with increasing transverse momentum, one finds in fact that the contribution of pions from resonances to the HBT signal decreases as p_{\perp} of the pions studied increases.

⁷ The calculation assumes that the pions from resonances are described by the same factorized form of the two-pion correlation function as the pions emerging directly from the collision volume. However, the pions from longer-lived resonances do not undergo any rescattering and thus reflect the statistics of the source resonances, which can in principle decrease the contribution to the HBT effect at small relative momenta.

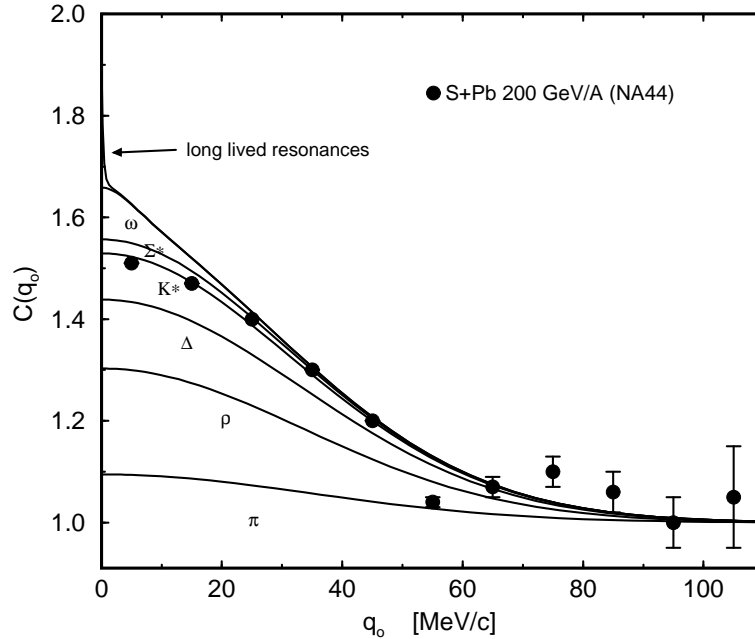


Fig. 12. Estimated contributions of pions from resonances in HBT compared with NA44 data [1]. From [36].

In the simple model of HBT described above we assumed well defined wave functions propagating through vacuum. But in reality the particles propagate through of order 1 mm of target and then, *e.g.*, in NA44, through 15 meters of air. Let us consider the effects of secondary scattering in the target and the intervening air. From a quantum mechanical point of view scattering from the target and air atoms changes an initial pure state wave function of a particle into a mixed quantum state: when a pure wave function hits the atoms in the target or air, it generates, à la Huygens, a beam of secondary wave functions; because the atoms are disturbed, the secondary waves become incoherent with the initial wave. The secondary interactions produce many small angle scatterings of the particles, which have the observational effect of distorting the correlation function [37].

To see the effects of small angle scattering, it is adequate to describe the interaction of a high energy particle with an atom of charge Z by a screened Coulomb potential, $V(r) = Ze^2 e^{-r/a}/r$, where $a = 0.8853a_0/Z^{1/3}$ is the Fermi–Thomas radius of the atom and a_0 is the Bohr radius, and neglect elastic scatterings due to strong interaction with the nucleus. The differential cross section of an incident particle of momentum p is given in

the Born approximation by

$$\frac{d\sigma}{d\Omega} = \frac{4p^2 Z(Z+1)\alpha^2}{(q^2 + \frac{1}{a^2})^2}, \tag{64}$$

where \vec{q} is the momentum transfer in the scattering, and the substitution $Z \rightarrow Z+1$ takes into account scattering by atomic electrons [38]. While the total cross section is $\sigma = 4\pi Z(Z+1)\alpha^2 a^2$, the effects of multiple scattering are more accurately controlled by the transport cross section,

$$\sigma_t \equiv \int d\Omega (1 - \cos\theta) \frac{d\sigma}{d\Omega},$$

given here by

$$\sigma_t = \frac{4\pi Z(Z+1)\alpha^2}{p^2} \left(\ln(2pa) - \frac{1}{2} \right). \tag{65}$$

In a single scattering, $\langle \cos\theta \rangle = 1 - \sigma_t/\sigma$, so that at high energies, $\langle \theta^2 \rangle \simeq 2\sigma_t/\sigma$.

Consider a particle going a distance L through a medium of atomic density n_a . From the multiple scattering equation one readily finds that the particle emerges with $\langle \cos\theta \rangle = e^{-n_a L \sigma_t}$, and more generally, with $\langle P_\ell(\cos\theta) \rangle = e^{-n_a L \sigma_\ell}$, where $\sigma_\ell = \int d\Omega (1 - P_\ell(\cos\theta)) d\sigma/d\Omega$ [39]. The underlying angular distribution is more complicated, but for our present estimates we may assume that the spread in angles is Gaussian: $f(\theta, L)\theta d\theta \sim e^{-\theta^2/\langle \theta^2 \rangle} \theta d\theta$. The mean square scattering angle $\langle \theta^2 \rangle$ is given by the non-linear equation [38],

$$\langle \theta^2 \rangle - \frac{4\pi Z(Z+1)\alpha^2}{p^2} n_a L \ln \langle \theta^2 \rangle = 2n_a L \sigma_t^{\text{eff}} \equiv \langle \theta^2 \rangle_0, \tag{66}$$

where

$$\sigma_t^{\text{eff}} = \frac{4\pi Z(Z+1)\alpha^2}{p^2} \ln \left(\frac{pa}{\nu^{1/2}} \right), \tag{67}$$

and the factor $\nu \approx 1.32(1 + 3.34Z^2\alpha^2)$ includes corrections to the cross section beyond the Born approximation. The second term on the left in Eq. (66) approximately takes into account effects of large angle scatterings, and reduces $\langle \theta^2 \rangle$ from $\langle \theta^2 \rangle_0$.

Let us consider as illustration the effect on a 4 GeV pion scattering through 1 mm of Pb. Then the mean scattering angle is $\sim 2 \times 10^{-3}$, which produces a mean transverse spread in momentum, Δp_\perp , of order 8 MeV, corresponding to a transverse deflection, Δr_\perp , of order 3 cm. Similarly, a 4

GeV pion traversing 15 m of air ($Z = 7$) undergoes a mean angular deflection $\sim 0.9 \times 10^{-3}$, with $\Delta p_{\perp} \sim 3.7$ MeV and $\Delta r_{\perp} \sim 1.4$ cm. The pion makes some 10^3 scatterings per cm; air is remarkably opaque to pions.

The effect of these small angle deviations is to spread out the singles distributions and the correlation function. Such secondary scattering effects are generally accounted for in the estimated experimental momentum resolution. An initial distribution of single particle transverse momenta, $n_{\vec{p}_{\perp}}^0$, will be spread into a final distribution,

$$n_{\vec{p}_{\perp}} \sim \int e^{-(\vec{p}_{\perp} - \vec{p}'_{\perp})^2 / \Delta p_{\perp}^2} n_{\vec{p}'_{\perp}}^0 d^2 \vec{p}'_{\perp}. \quad (68)$$

Similarly, two particles starting out with a given relative momentum and undergoing random walks do not end up with the same final relative momentum. For example, two particles detected with zero relative momentum may have actually started out at a larger momenta and have been bent in by the air or target. An initial HBT correlation function $C_0(q) = 1 + e^{-\vec{q}^2 R_0^2}$ will be spread into an observed correlation function,

$$C_{\text{obs}}(q) = 1 + \lambda_{\text{eff}} e^{-\vec{q}^2 R_{\text{eff}}^2}, \quad (69)$$

where the measured radius R_{eff} is decreased from the original radius, R , by a factor

$$\frac{R_{\text{eff}}}{R} = \frac{1}{[1 + 2(R\Delta p_{\perp})^2]^{1/2}}, \quad (70)$$

and the chaoticity parameter is reduced from unity to

$$\lambda_{\text{eff}} = \left(\frac{R_{\text{eff}}}{R} \right)^2. \quad (71)$$

For example, with an initial nominal radius of $R = 7$ fm, scattering in air reduces the measured R by 2% and the measured λ by 3%. Including the effect of a 1 mm Pb target, one finds a 7% reduction in the measured R and a total reduction of λ due to secondary scattering of 16%. The effects on HBT of secondary scattering in a thick target can be substantial; *e.g.*, for 1 cm of Pb, λ falls below 0.4.

The astute reader may at this point have noticed a contradiction between the picture of secondary scattering in a cloud obscuring a smaller source, the sun say, leading to a narrower correlation function than the one that would be produced by the sun (*cf.* Fig. 7(c)), and the present picture of scattering in air, which broadens the correlation function and reduces it at the origin. I leave the resolution of this problem as an instructive exercise.

9. Final state Coulomb interactions

Up to now we have discussed Hanbury Brown–Twiss interferometry assuming that the particles travel completely independently once they leave the collision region. In fact one measures correlations primarily among charged mesons; the Coulomb interactions between any given pair of particles, as well as those of the individuals in the pair with the other charged particles in the system, produce important effects on the measured correlation functions. Even though the detectors are many meters from the collision, those that produce the enhanced signal are typically within a meter of each other. The pions whose correlation one measures travel essentially along the same direction and they continue to have a strong Coulomb interaction the entire way. Disentangling these final state Coulomb interactions is a very difficult question⁸.

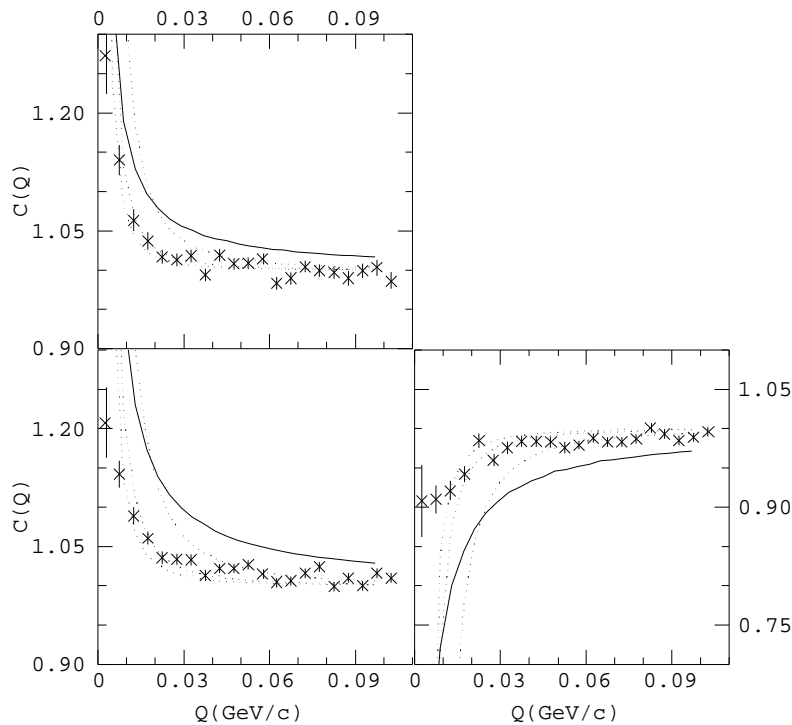


Fig. 13. E877 data [41] for (a) $\pi^+\pi^-$, (b) π^-p , and (c) π^+p , as well as comparison (dotted lines) with the toy model, Eq. (78) for r_0 in the range 3–15 fm, assuming a bare correlation function $C_0 = 1$, and the Gamow correction (solid line).

⁸ Most of the material described in this Section was developed by the author and P. Braun–Munzinger, with J. Popp’s helpful assistance, and reported in Ref. [40].

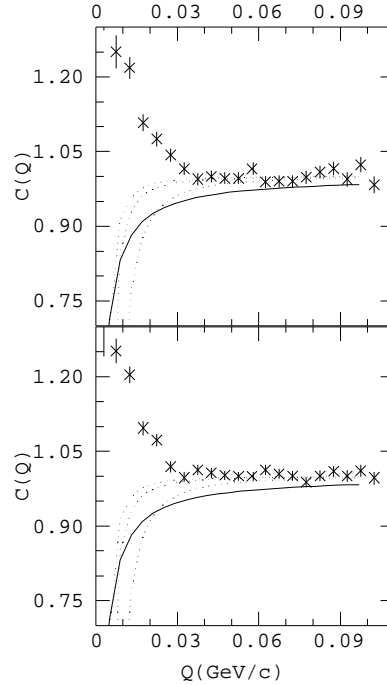


Fig. 14. E877 data [41] for $\pi^+\pi^+$ and (b) $\pi^-\pi^-$, together with the Coulomb correction, Eq. (78), for the same range of r_0 as in Fig. 13.

Bare data, uncorrected for Coulomb interactions, brings out the situation very clearly. Figure 13 shows the uncorrected E877 correlation function measurements for $\pi^+\pi^-$, π^-p , and π^+p pairs produced in Au+Au collisions at the AGS at 10.8 GeV per nucleon [41], while Fig. 14 shows bare data for the $\pi^+\pi^+$ and $\pi^-\pi^-$ correlation functions. The correlation function for distinguishable particle pairs does not have the expected value of unity, while the correlation function for identical particles does not rise up anywhere as high as in the Coulomb-corrected data, *e.g.*, Figs 1, 2, and 9–11. Rather, the data for both identical particles and oppositely charged non-identical particles are very similar.

The traditional method of correcting for final state Coulomb interactions is to employ the Gamow correction. For example, in the beta decay of a neutron into a proton, electron, and antineutrino, the proton and electron are produced in a relative Coulomb state. Because the electron and proton are attracted to each other, the amplitude for them to be at the origin is enhanced. The decay amplitude is a bare matrix element times the relative electron–proton Coulomb wave function, $\psi_C(0)$, at the origin. Non-relativistically, the Coulomb wave function for the relative mo-

tion of a pair of particles of charges ze and $z'e$ with relative momentum $\vec{Q} = (\vec{p} - \vec{p}')/2 = \vec{q}/2$ at infinity, and relative velocity $v_{\text{rel}} = Q/m_{\text{red}}$, is $\psi_C(\vec{r}) = \psi_C(0) {}_1F_1(-i\eta; 1; i(Qr - \vec{Q} \cdot \vec{r}))$, where the dimensionless parameter $\eta(Q)$ is given by

$$\eta = \frac{zz'\alpha}{v_{\text{rel}}/c}, \quad (72)$$

and the reduced mass m_{red} equals $m/2$ for two particles of mass m . Also,

$$\psi_C(0) = \left(\frac{2\pi\eta}{e^{2\pi\eta} - 1} \right)^{1/2}. \quad (73)$$

The actual rate is that which one would measure in the absence of any Coulomb effects times the Coulomb correction, $|\psi_C(0)|^2$. For particles of opposite charge the probability is enhanced, by a factor tending to $2\pi|\eta|$ at small Q . On the other hand imagine a decay of a Δ^{++} into a proton, positron and neutrino. The proton and positron repel each other, and thus have a reduced amplitude to be at the origin. The Coulomb correction, $|\psi_C(0)|^2$, is less than unity in this case, and the net rate would be suppressed from its value in the absence of Coulomb interactions, by a factor tending to $2\pi\eta e^{-2\pi\eta}$ at small Q .

In making a Gamow correction in heavy-ion collisions, one assumes that the pair of identical particles is produced in a relative Coulomb state at zero separation, and thus the amplitude for doing so is reduced from the bare amplitude by the factor $\psi_C(0)$. The *bare* correlation function, $C_0(q)$, where $q = 2Q$, is thus extracted from the measured correlation function, $C(q)$, by dividing out the assumed factor $|\psi_C(0)|^2$ in the production rate:

$$C_0(q) = \frac{C(q)}{|\psi_C(0)|^2} = C(q) \frac{(e^{2\pi\eta(Q)} - 1)}{2\pi\eta(Q)}. \quad (74)$$

Note that as the relative momentum goes to zero, $\eta \rightarrow +\infty$ and $\psi_C(0) \rightarrow 0$ for identical particles, and Eq. (74) yields an infinite correction.

The question is why one should assume that the Coulomb wave function at the origin should control the Coulomb corrections? For particles of the same charge, $\psi_C(r)$ falls to zero exponentially as the particles approach each other inside the (zero angular momentum) *classical turning point*, r_t , defined by $q^2/2m_{\text{red}} = e^2/r_t$. Outside r_t it oscillates, and describes essentially classical physics. In order for the physics at the origin to be relevant, it is necessary that the source be highly localized compared to the distance to the turning point. However, for pions in a heavy-ion collision, $r_t \simeq (200 \text{ fm})/Q^2$, where Q is measured in MeV/c ; for $Q \sim 10 \text{ MeV}/c$, a typical minimum value, r_t is only 2 fm, and smaller for larger Q . Since r_t is much smaller

than the characteristic heavy-ion radius, most of the pairs of particles observed in a heavy-ion collision are in fact made at relative separations well outside their classical turning points.

There are three relevant length scales in the Coulomb problem, the classical turning point, r_t , the wavelength of the relative motion, and the two-particle Bohr radius, $a_0 = 1/m_{\text{red}}e^2$ (which is 387 fm for $\pi\pi$ and 222 fm for πp). For typical Q , these length scales are cleanly separated:

$$r_t : 1/Q : a_0 = 2 : a_0Q : (a_0Q)^2. \quad (75)$$

For $\pi\pi$ (or πp), $a_0Q = 1/|\eta| = 1.96$ (or 1.13) $Q/(\text{Mev}/c) \gg 1$. The classical turning point is thus the relevant scale for Coulomb effects. These arguments suggest that the Coulomb corrections are dominated by classical physics.

The major effect of the Coulomb interaction between the particles in the pair, at distances large compared with r_t , is to accelerate them relative to each other. Particles of the same charge are accelerated to larger relative momenta, thus depressing the observed distribution at small Q , while particles of opposite charge are reduced in relative momentum in the final state, which builds up the distribution at small Q . Although these effects are qualitatively similar those produced by the Gamow correction, they are quantitatively rather different.

In the presence of many produced particles, the relative motion of the particles in the pair is strongly affected by their interactions with the plasma of other particles. The mutual Coulomb interaction of the pair becomes dominant only when the pair has sufficiently separated from the other particles in the system that there is small probability of finding other particles between the particles in the pair.

One can write down a simple toy model to take these effects into account, by simply neglecting the Coulomb interaction between the pair for separations less than an initial radius r_0 , and for separations greater than r_0 including only the relative Coulomb interaction. Since the relative motion is in the classical region, conservation of energy of the pair implies that the final observed relative momentum Q is related to the initial momentum of the pair Q_0 at r_0 by

$$\frac{Q^2}{2m_{\text{red}}} = \frac{Q_0^2}{2m_{\text{red}}} \pm \frac{e^2}{r_0}, \quad (76)$$

where the upper sign is for particles of like charge, and the lower for particles of opposite charge. For example, for pions with $r_0 = 10$ fm, $Q^2 = Q_0^2 \pm 20(\text{MeV}/c)^2$. The physics can be treated non-relativistically because in the rest frame of the pair, one is interested in relative momenta small compared with mc .

Since the Coulomb interaction conserves particles and the total momentum of the pair, the final distribution d^6n/d^3pd^3p' of relative momenta Q is thus given in terms of the initial distribution of pairs, $d^6n^0/d^3p_0d^3p'_0$, by

$$\frac{d^6n}{d^3pd^3p'}d^3Q = \frac{d^6n^0}{d^3p_0d^3p'_0}d^3Q_0. \quad (77)$$

The Jacobian, with changes in relative angles ignored, is, from Eq. (76), $d^3Q_0/d^3Q = Q_0/Q$. Neglecting to good accuracy the effects of Coulomb interactions on the singles distributions we have

$$C(\vec{q}) = \frac{q_0}{q}C_0(\vec{q}_0) = \left(1 \mp \frac{2m_{\text{red}}e^2}{r_0Q^2}\right)^{1/2} C_0(\vec{q}_0). \quad (78)$$

Figure 13 compares the predictions of the toy model, Eq. (78), with the E877 data for $\pi^+\pi^-$, π^-p , and π^+p systems in Au+Au collisions at the AGS [41], assuming that the bare correlation function C_0 equals unity. The dashed lines are the results of the toy model for $r_0 = 3$ fm (rightmost curve), 9 fm, and 15 fm (leftmost curve), along with the standard Gamow correction (solid line). Except at very small relative momenta $Q \lesssim 10$ MeV/c, where effects due to the finite momentum resolution of the experiment become visible in the data, the model gives a good account of the data for r_0 in the range of 9–15 fm. By contrast, the Gamow factor considerably overpredicts the data for all Q shown here. Similar bare data from NA49 at CERN, for $\pi^+\pi^-$ produced in 160 GeV per nucleon Pb on Pb collisions is also well fit by the toy model with $r_0 \sim 10 - 20$ fm, while again the Gamow correction is too large, as in Fig. 13 [42].

Note that the raw correlation data for non-identical particles contains information about the mean separation of pairs when screening effects become negligible, summarized in the toy model by the parameter r_0 , which is possibly Q dependent.

With the initial radius r_0 extracted from the unlike-sign data, one can then construct the Coulomb correction for like-sign particles. The Coulomb correction factor deduced from Eq. (78) is shown for $\pi^+\pi^+$ in Fig. 14(a) and $\pi^-\pi^-$ in Fig. 14(b), for the same range of r_0 (as in Fig. 13, the rightmost curve corresponds to $r_0 = 3$ fm). Again we see that use of the Gamow factor implies a correction which differs significantly from that of the toy model.

Dividing the raw E877 data by the toy model correction factor, with $r_0 = 15$ fm, we obtain the correlation function for like-sign pions (crosses) shown in Fig. 15(a) for $\pi^+\pi^+$ and Fig. 15(b) for $\pi^-\pi^-$, which also shows the correlation function (vertical bars) derived by making the standard Gamow correction. Using the Gamow factor instead of the proper Coulomb correction

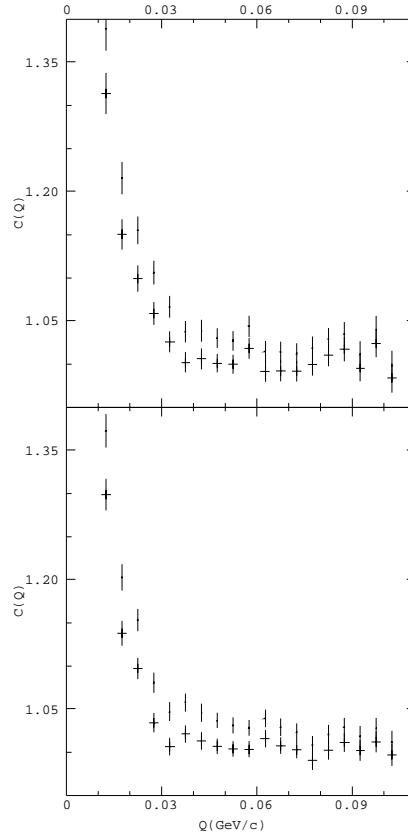


Fig. 15. Toy model calculation of $C(Q)$ for like-sign pions (crosses), compared with the correlation function derived by making the standard Gamow correction (vertical bars); (a) $\pi^+\pi^+$ and (b) $\pi^-\pi^-$.

leads to a correlation function which is $\sim 30\%$ wider, implying a correspondingly reduced radius parameter. Furthermore, the shape of the “Gamow-corrected” correlation functions have considerable non-Gaussian tails in the range $30 < Q < 80$ MeV/ c . These tails do not exist in the raw correlation function and obscure the interpretation of the data.

The length r_0 gives one a measure of the scale at which Coulomb interactions between the particles in the pair dominate their relative motion. To calculate this decoupling length from microscopic models requires a non-trivial description of many-particle screening in the high frequency regime. The Coulomb corrections will furthermore change character at RHIC energies, where the meson density in given events will be sufficiently large that the Coulomb corrections remain those of a many-particle system out to much larger distances.

In order to make a bridge between the toy model and the Gamow correction, as a first step in constructing a more accurate accounting of Coulomb corrections, it is instructive to review how the classical description emerges from the full quantum-mechanical treatment of the Coulomb problem. In the absence of Coulomb interactions (denoted by 0 here) the number of pairs of relative momentum \vec{Q} is given by Eq. (34):

$$\varepsilon_p \varepsilon'_p \left(\frac{d^6 n}{d^3 p d^3 p'} \right)_0 = \frac{1}{4} \int dx dx' dx'' dx''' e^{iP(x+x''-x'-x''')/2} e^{iQ(x-x''-x'+x''')} \times \langle J^\dagger(x) J^\dagger(x'') J(x''') J(x') \rangle. \quad (79)$$

To take into account the Coulomb interaction only between the pair of produced particles, we simply replace the relative free-particle wave functions, $e^{iQ(x-x')}$ and $e^{iQ(x'-x''')}$, by the Coulomb wave functions, $\psi_C(x-x'')$ and $\psi_C(x'-x''')$ for the relative motion for a pair of relative momentum Q at infinity, so that

$$\varepsilon_p \varepsilon'_p \frac{d^6 n}{d^3 p d^3 p'} = \frac{1}{4} \int dx dx' dx'' dx''' e^{iP(x+x''-x'-x''')/2} \psi_C(x-x'') \psi_C^*(x'-x''') \times \langle J^\dagger(x) J^\dagger(x'') J(x''') J(x') \rangle. \quad (80)$$

Pairs of low relative momentum have relatively low angular momentum, *e.g.*, a pair produced at 10 fm separation with relative momentum 20 MeV/ c can have at most one unit of relative angular momentum. Thus only the low partial wave components of the Coulomb wave function enter Eq. (80) with appreciable probability. Let us consider just s-waves in the WKB approximation, which is quite good for the s-wave outside the collision volume⁹. Outside the classical turning point the s-wave is

$$\psi_C^s(r) \simeq \frac{1}{rk(r)^{1/2} Q^{1/2}} \sin \phi(r), \quad (81)$$

where the local relative momentum, measuring the rate of change of phase, ϕ , of the wave function, is given by

$$k(r) = \frac{d\phi}{dr} = \left(Q^2 \mp \frac{2m_{\text{red}} e^2}{r} \right)^{1/2}. \quad (82)$$

⁹ The condition for validity of the approximation is $|\partial p(r)/\partial r| \ll p(r)^2$, which for $r \ll a_0$, the region of interest, becomes the restriction, $r \gtrsim 3/q^{3/2} a_0^{1/2}$. For $\pi\pi$ (or πp) pairs with $Q > 20$ MeV/ c , WKB is reasonable for r down to ~ 5 fm (or ~ 6 fm).

(Equation (81), with ℓ -dependent $\phi(r)$ holds as well for higher partial waves, $\ell > 0$.) The normalization of (81) agrees with (73) as $r \rightarrow 0$, while as $r \rightarrow \infty$, the Coulomb wave function behaves as

$$\psi_C^s(r) \rightarrow \frac{1}{Qr} \sin(Qr - \eta \ln 2Qr + \delta_0). \quad (83)$$

The distribution of s-wave pairs in the absence of Coulomb interactions is

$$\begin{aligned} \varepsilon_p \varepsilon'_p \left(\frac{d^6 n}{d^3 p d^3 p'} \right)_0^s &= \frac{1}{4} \int dx dx' dx'' dx''' e^{iP(x+x''-x'-x''')/2} \\ &\times \frac{\sin Q|r-r''|}{Q|r-r''|} \frac{\sin Q|r'-r'''}{Q|r''-r'''} \langle J^\dagger(x) J^\dagger(x'') J(x''') J(x') \rangle. \end{aligned} \quad (84)$$

Then since in the region of any radius r outside the turning point the Coulomb wave function behaves locally as a free particle s-wave of momentum $k(r)$, the s-wave pair distribution function is given by

$$\left(\frac{d^6 n}{d^3 p d^3 p'} \right)_0^s \approx \frac{k(r_0)}{Q} \left(\frac{d^6 n}{d^3 p d^3 p'} \right)_0, \quad (85)$$

where the factor $k(r_0)/Q$ arises from the denominators in Eqs (81) and (84). Consequently, $C(q) \simeq C_0(k(r_0))k(r_0)/Q$, the result in Eq. (78) with $Q_0 = k(r_0)$. Doing classical physics using Coulomb wave functions is again using a steam roller to crack a nut.

With the connection between the toy model and the Coulomb wave function we can now extend the description of Coulomb corrections to smaller values of the source radius r_0 . In general, the effect of the Coulomb interactions depends on the detailed structure of the source correlation function; let us describe the localization of the source correlation function $\langle J^\dagger(x) J^\dagger(x'') J(x''') J(x') \rangle$ in both $|\vec{r} - \vec{r}''|$ and $|\vec{r}' - \vec{r}'''|$ by writing

$$\begin{aligned} \langle J^\dagger(x) J^\dagger(x'') J(x''') J(x') \rangle &\approx s(x-x'') s(x'-x''') \\ &\times (\langle J^\dagger(x) J(x') \rangle_0 \langle J^\dagger(x'') J(x''') \rangle_0 \\ &+ \langle J^\dagger(x) J(x''') \rangle_0 \langle J^\dagger(x'') J(x') \rangle_0), \end{aligned} \quad (86)$$

where $s(x-x')$ defines the effective initial separation of the pair. For small relative momenta, the combination $\psi_C(x)s(x) \equiv f(x)$ varies slowly on a scale of the coherence length ξ_c . Then we find, roughly,

$$\begin{aligned} \varepsilon_p \varepsilon'_p \frac{d^6 n}{d^3 p d^3 p'} &= \frac{1}{4} \int dx dx' dx'' dx''' f(w) (f^*(w) + f^*(-w)) e^{iP(x+x''-x'-x''')/2} \\ &\times \langle J^\dagger(x) J(x') \rangle_0 \langle J^\dagger(x'') J(x''') \rangle_0, \end{aligned} \quad (87)$$

where $w = (x - x' + x''' - x'')/2$. The integrals in this equation are sufficiently involved that the Coulomb corrections would have to be extracted numerically. However, if as an approximation we simply replace the term $f(w)(f(w) + f(-w))$ by its integral over all space, we arrive basically at Pratt's formula [43]:

$$C(Q) \simeq \int d^3r (|f(r)|^2 + f(r)f^*(-r))C_0(Q), \tag{88}$$

for the modification of the correlation function by Coulomb interactions.

The correction to the direct term in Eq. (88) has the form

$$C(Q)_{\text{dir}} = \int |\psi_C(r)|^2 |s(r)|^2. \tag{89}$$

To illustrate the transition from the Gamow correction to the toy model let us take $|s(r)|^2$ to be a normalized Gaussian of range r_0 : $|s(r)|^2 = (2\pi)^{-3/2} r_0^{-3} \exp(-r^2/2r_0^2)$. We show, in Fig. 16, for the $\pi^+\pi^-$ system, the results of calculations of the correction term $\int |\psi_C(r)|^2 |s(r)|^2$ for $r_0 = 1, 5, 9,$ and 18 fm (dash-dot curves, the highest for $r_0 = 1$ fm, and falling with increasing r_0). As $r_0 \rightarrow 0$, the projection of the square of the Coulomb wave function onto the source $|s(r)|^2$ converges to the standard Gamow correction (solid line); for $r_0 < 0.1$ fm (not shown in Fig. 16) the difference between the Gamow correction and a calculation with Eq. (89) is less than 0.5%. For larger r_0 values the correction rather quickly approaches the prediction of the toy model (shown here for an initial radius of 9 fm as a dotted curve), indicating that, for pairs originating outside their classical turning point, the toy model provides an adequate and reasonably accurate description of the Coulomb effects.

Let us turn next to the question of the effects of the Coulomb interactions of the pair with the remaining particles. This is a difficult many-body problem, which we greatly simplify as a first approximation by assuming that the remaining particles can be described by a central Coulomb potential, $Z_{\text{eff}}e^2/r$, where in a central collision of nucleus A with nucleus B the effective charge Z_{eff} is of order of the total initial nuclear charge ($Z_A + Z_B$). This central potential accelerates positive mesons away and slows down the negatives, effects described by the Coulomb wave functions for the potential. The final momentum of any particle is related to the initial momentum p_a at production point r_a by

$$\epsilon(p) = \epsilon(p_a) \pm \frac{Z_{\text{eff}}e^2}{r_a}, \tag{90}$$

where $\epsilon(p) = (p^2 + m^2)^{1/2}$. (While Coulomb effects for the relative momentum can be treated non-relativistically as in Eq. (76), the individual

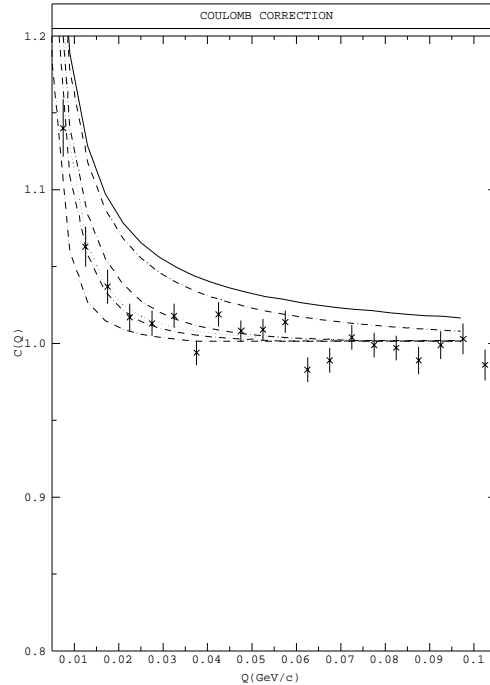


Fig. 16. Transition from the toy model (dotted line, with $r_0 = 9$ fm) to the Gamow correction (solid line) with decreasing source size, calculated from Eq. (89) (dash-dot curves). From highest to lowest dash-dot curves the source range r_0 is 1, 5, 9, and 18 fm.

momenta are generally relativistic.) For simplicity let us ignore quantum mechanical suppressions or enhancements of the amplitude for particle emission, as well as possible effects of angular changes in the individual particle orbits on the particle distributions. Then the single particle distribution is modified by the central potential, analogously to Eq. (77), by

$$\frac{d^3 n(\vec{p})}{d^3 p} = \frac{d^3 n_0(\vec{p}_a)}{d^3 p_a} \frac{d^3 p_a}{d^3 p} = \frac{p_a \epsilon(p_a)}{p \epsilon(p)} \frac{d^3 n_0(\vec{p}_a)}{d^3 p_a}. \quad (91)$$

Both the magnitude of the distribution as well as its argument are shifted. Experimental observation of these effects is reported in Ref. [44].

Although the central potential shifts the singles distribution, it cannot introduce any correlations among emitted particles that have no initial correlation in the absence of the central potential, *e.g.*, as one usually assumes for different species or oppositely charged pions. If in the absence of the central potential, uncorrelated particles [$C(Q) = 1$] are emitted in independent free particle states, then in the presence of the poten-

tial they are emitted in Coulomb states for the central potential, but still $d^6n(\vec{p}, \vec{p}')/d^3pd^3p' = (d^3n(\vec{p})/d^3p)(d^3n(\vec{p}')/d^3p')$ and $C(Q)$ remains unity.

For particles that are initially correlated as a consequence of Bose–Einstein statistics, $d^6n(\vec{p}, \vec{p}')/dp^3dp'^3$ and $(d^3n(\vec{p})/dp^3)(d^3n(\vec{p}')/dp'^3)$ will be modified both by the Jacobians of the transformations from initial to final momenta, and shifts of argument. However, in forming $C(q)$, the effects of the Jacobians in the numerator and denominator essentially cancel, and the primary effect is the shift in the arguments:

$$C(\vec{q}) = \frac{\{d^6n_2(\vec{p}_a, \vec{p}_a')d^3p_ad^3p'_a\}}{\left\{\frac{d^3n(\vec{p}_a)}{d^3p_a} \frac{d^3n(\vec{p}_a')}{d^3p'_a}\right\}}. \quad (92)$$

Since positive particles are accelerated, the final momentum difference, $\vec{q} = \vec{p} - \vec{p}'$, of a positive pair will generally be larger in magnitude than it is initially, while for negative pairs the final momentum difference will generally be smaller. Thus we expect the central Coulomb potential to cause the size of the collision volume extracted from positive pairs to be smaller than the actual size, and that from negative pairs to be larger than the actual size. As an illustration consider a pair of relativistic particles whose initial momenta \vec{p}_a and \vec{p}_a' are equal in magnitude to p_a , and final momenta \vec{p} and \vec{p}' equal in magnitude to p ; then

$$q = \left(\frac{p}{p_a}\right) q_a \simeq q_a \left(1 \pm \frac{Z_{\text{eff}}e^2/r_a}{p_a}\right), \quad (93)$$

where the upper sign refers to both particles positively charged and the lower to both negatively charged. For $Z \sim 150$, $r_a \sim 7$ fm and $p_a \sim 300$ MeV/ c , the effect is an increase for positives (and a decrease for negatives) in the observed scale of $C(Q)$ and decrease (or increase) in the extracted radius of ten percent. Such a shift of the same magnitude has been observed by E877 in 10.8 GeV/ A collisions of Au on Au [41]; however, NA44 recently reports an effect in the opposite direction, in 158 GeV/ A Pb on Pb collisions, in radii as a function of charged particle multiplicity [33], indicating the need for a more refined theory of the effect of the central Coulomb potential [45].

10. Applications in condensed matter and atomic physics

Let me finally mention briefly work on HBT in condensed matter and atomic physics. Recently, Yasuda and Shimizu (at Tokyo University) [22] have made the first measurement of HBT correlations in an atomic system, observing the time correlations in laser-cooled ultracold (but not yet Bose–Einstein condensed) beams of bosonic ^{20}Ne atoms. The correlations in the

beam are those expected from a thermal source, where the correlation time is the inverse of the temperature of the beam. Indeed the HBT correlation function begins to rise at time separations less than $\sim 0.5 \times 10^{-6}$ sec to a value a factor of two larger than at large time, corresponding to a beam temperature $\sim 10^2 \mu\text{K}$. This result is very similar to the original Hanbury Brown–Twiss tabletop experiment on photon bunching from a Hg vapor lamp. By contrast, a measurement of HBT correlations in the MIT atomic laser [35] would yield no such atomic bunching, because of the coherence of the beam, but rather the correlation function would remain flat. Lack of an HBT enhancement would indicate coherence of the beam. In general, loss of HBT correlations would probe the onset of Bose–Einstein condensation, not only in atomic systems, but in condensed matter systems such as the observed Bose-condensed paraexcitons in cuprous oxide [46, 47].

Another interesting application of HBT has been in light scattering from atoms trapped in optical lattices [48]. Jurczak *et al.* (at Orsay) have created an optical lattice with an arrangement of four lasers in which they trap atomic rubidium at a density $\sim 2 \times 10^9 \text{ cm}^{-3}$, filling about 10^{-4} of the lattice sites. The lasers also scatter from the rubidium, and the time correlations in the scattered light (of two different polarizations) effectively measure the atom–atom correlation functions in the lattice. From these measurements they are able to measure the diffusion of the loosely packed atoms in the optical lattice. Lastly we mention that HBT has also been proposed as a probe of the space and time structure of bubbles in sonoluminescence [49].

In summary, the technique of Hanbury Brown and Twiss, which was first developed to measure astronomical object of sizes at least 10^{12} cm, has, as we have seen, turned into a valuable tool to measure subatomic phenomena on the quite opposite scale of 10^{-12} cm. More recent experiments have shown its utility in atomic and condensed matter physics as well. While the basic theory underlying the nuclear applications is established, as described in these lectures, many effects, *e.g.*, Coulomb interactions, possible non-chaoticity, non-zero coherence lengths, multiple scattering, *etc.*, introduce various levels of uncertainty into the interpretation of the HBT measurements. A better understanding of such effects remains a challenge in an accurate connection of HBT measurements to the microscopic physics of collisions.

These lectures are a small birthday tribute to my dear friend Wiesław Czyż who over the years opened many worlds to me — from Zakopane and Cracow, to the pleasures of high energy nuclear physics. I would like to take this opportunity to express my gratitude to the organizers of the present Cracow School of Theoretical Physics at Zakopane for enabling me to participate in the School where these lectures were given. I would also

like thank the members of my group in Urbana — Alejandro Ayala, James Popp, and Benoit Vanderheyden — who are responsible for much of the material reported here, and Michael Baym for preparing the graphics. I am also grateful to Peter Braun–Munzinger, Henning Heiselberg, Barbara Jacak, and Dariusz Miskowiec for many discussions of this material and for making figures available, and to Ulrich Heinz for insightful comments on the manuscript. This work was supported in part by U.S. National Science Foundation Grant No. PHY94-21309.

REFERENCES

- [1] H. Bøggild *et al.*, NA44 collaboration, *Phys. Lett.* **B302**, 510 (1993); **B349**, 386 (1995).
- [2] D. Miskowiec *et al.*, E877 collaboration, *Nucl. Phys.* **A610**, 237c (1996).
- [3] B.V. Jacak, *Nucl. Phys.* **A590**, 215c (1995).
- [4] D. Boal, C.K. Gelbke, B. Jennings, *Rev. Mod. Phys.* **62**, 553 (1990).
- [5] W. Bauer, C. Gelbke, S. Pratt, *Ann. Rev. Nucl. Part. Sci.* **42**, 77 (1992), and references therein.
- [6] U. Heinz, *Nucl. Phys.* **A610**, 264c (1996).
- [7] S. Pratt, Proc. 13th Int. Conf. on Nucleus–Nucleus Collisions, QM97, *Nucl. Phys.* **A**, in press.
- [8] B.V. Jacak, *Rev. Mod. Phys.* (1998), in press.
- [9] G. Baym, *Lectures on Quantum Mechanics* (W.A. Benjamin, Inc., New York, 1969), pp. 431-434.
- [10] R. Hanbury Brown, *Boffin*, Adam Hilger, Bristol 1991, pp.104-105.
- [11] Op. cit., p. 108.
- [12] R. Hanbury Brown, R.Q. Twiss, *Phil. Mag., Ser. 7* **45**, 663 (1954).
- [13] R. Hanbury Brown, R.Q. Twiss, *Nature* **177**, 27 (1956).
- [14] E. Purcell, *Nature* **178**, 1449 (1956).
- [15] R. Hanbury Brown, R.Q. Twiss, *Nature* **178**, 1046 (1956).
- [16] G. Goldhaber, S. Goldhaber, W. Lee, A. Pais, *Phys. Rev.* **120**, 300 (1960).
- [17] Private communication, July 1997.
- [18] N.M. Agababyan *et al.*, NA22 collaboration, *Z. Phys.* **C71**, 409 (1996).
- [19] P.D. Acton *et al.*, OPAL collaboration, *Phys. Lett.* **B267**, 143 (1991); *Z. Phys.* **C58**, 207 (1993); P. Abreu *et al.*, DELPHI collaboration, *Phys. Lett.* **B286**, 201 (1992); D. Decamp *et al.* (ALEPH), *Z. Phys.* **C54**, 75 (1992).
- [20] R.P. Feynman, *Theory of Fundamental Processes*, W.A. Benjamin, Inc., New York 1961, p. 6.
- [21] R. Ghetti *et al.*, *Nucl. Inst. Methods Phys. Res.* **A335**, 156 (1993).
- [22] M. Yasuda, F. Shimizu, *Phys. Rev. Lett.* **77**, 3090 (1996).

- [23] J. Popp, Ph.D. thesis, University of Illinois, 1997 (unpublished).
- [24] A. Ayala, G. Baym, J. Popp, *Nucl. Phys. A*, to be published.
- [25] S. Pratt, *Phys. Rev. Lett.* **53**, 1219 (1984).
- [26] F.B. Yano, S.E. Koonin, *Phys. Lett.* **B78**, 556 (1978).
- [27] M.I. Podgoretskii, *Yad. Fizika* **37**, 455 (1983) [Engl. trans., *Sov. J. Nucl. Phys.* **37**, 272 (1983)].
- [28] S. Chapman, P. Scotto, U. Heinz, *Phys. Rev. Lett.* **74**, 4400 (1995).
- [29] H. Bøggild *et al.*, NA44 Collaboration, *Phys. Lett.* **B349**, 386 (1995).
- [30] J. Barrette *et al.*, E877 collaboration, *Phys. Rev. Lett.* **78**, 2916 (1997).
- [31] S.A. Voloshin, W.E. Cleland, *Phys. Rev.* **C54**, 3212 (1996).
- [32] U. Heinz, B. Tomasik, U.A. Wiedemann, Y.-F. Wu, *Phys. Lett.* **B382**, 181 (1996).
- [33] A. Sakaguchi, NA44 collaboration, Proc. 13th Int. Conf. on Nucleus–Nucleus Collisions, QM97, *Nucl. Phys. A*, in press.
- [34] J.D. Bjorken, K. Kowalsky, C.C. Taylor, SLAC-PUB-6109 (1993); K. Rajagopal, F. Wilczek, *Nucl. Phys.* **B379**, 395 (1993); S. Gavin, *Nucl. Phys.* **A590**, 163c (1995); J.D. Bjorken, *Acta Phys. Pol.* **B28**, 2773 (1997).
- [35] M.-O. Mewes, M.R. Andrews, D.M. Kurn, D.S. Durfee, C.G. Townsend, W. Ketterle, *Phys. Rev. Lett.* **78**, 582 (1997).
- [36] H. Heiselberg, *Phys. Lett.* **B379**, 27 (1996).
- [37] A. Ayala, G. Baym, B.V. Jacak, J. Popp, B. Vanderheyden, to be published.
- [38] H.A. Bethe, *Phys. Rev.* **89**, 1256 (1953).
- [39] S.A. Goudsmit, J.L. Saunderson, *Phys. Rev.* **57**, 24 (1940); **58**, 36 (1940).
- [40] G. Baym, P. Braun-Munzinger, *Nucl. Phys.* **A610**, 286c (1996).
- [41] D. Miskowicz, E877 collaboration, *Nucl. Phys.* **A590**, 473c (1995).
- [42] K. Kadija, NA49 collaboration, *Nucl. Phys.* **A610**, 248c (1996), and H. Ströbele, private communication.
- [43] S. Pratt, *Phys. Rev.* **D33**, 72 (1986).
- [44] H. Bøggild *et al.*, NA44 collaboration, *Phys. Lett.* **B372**, 339 (1996).
- [45] D. Hardtke, Ph.D. thesis, Ohio State University, 1997 (unpublished).
- [46] D.W. Snoke, J.P. Wolfe, A. Mysyrowicz, *Phys. Rev. Lett.* **59**, 827 (1987); J.-L. Lin, J.P. Wolfe, *Phys. Rev. Lett.* **71**, 1223 (1993).
- [47] G.M. Kavoulakis, G. Baym, J.P. Wolfe, *Phys. Rev.* **B53**, 1 (1996).
- [48] C. Jurczak, B. Desruelle, K. Sengstock, J.-Y. Courtois, C.I. Westbrook, A. Aspect, *Phys. Rev. Lett.* **77**, 1727 (1996); C.I. Westbrook, C. Jurczak, G. Birkel, B. Desruelle, W.D. Phillips, A. Aspect, *J. Mod. Opt.* **44**, 1837 (1997).
- [49] S. Trentalange, S.U. Pandey, *J. Acoust. Soc. Am.* **99**, 2439 (1996); Y. Hama, T. Kodama, S. Padula, quant-ph/9612046; C. Slotta, U. Heinz, quant-ph/9711058; H.-Th. Elze, T. Kodama, J. Rafelski, cond-mat/9712097.